General Disclaimer

One or more of the Following Statements may affect this Document

- This document has been reproduced from the best copy furnished by the organizational source. It is being released in the interest of making available as much information as possible.

- This document may contain data, which exceeds the sheet parameters. It was furnished in this condition by the organizational source and is the best copy available.

- This document may contain tone-on-tone or color graphs, charts and/or pictures, which have been reproduced in black and white.

- This document is paginated as submitted by the original source.

- Portions of this document are not fully legible due to the historical nature of some of the material. However, it is the best reproduction available from the original submission.

Produced by the NASA Center for Aerospace Information (CASI)

DRA

LMSC-HREC TR D867640

MANUFACTURING IN SPACE: FLUID DYNAMICS NUMERICAL ANALYSIS

September 1982

Contract NASW-3281 (Annual Report)

Prepared for

NASA HEADQUARTERS
WASHINGTON, DC 20546

by

S. J. Robertson
L. A. Nicholson
L. W. Spradley

Lockheed
Missiles & Space Company, Inc.
Huntsville Research & Engineering Center
4800 Bradford Drive, Huntsville, AL 35807

(NASA-CR-169536) MANUFACTURING IN SPACE: FLUID DYNAMICS NUMERICAL ANALYSIS Annual Report (Lockheed Missiles and Space Co.) 84 p HC A05/MF A01 CSCL 22A N83-13129
Unclas
G3/12 01092

FOREWORD

This document is an annual report describing the results of effort by personnel of Lockheed Missiles & Space Company, Inc., Huntsville Research & Engineering Center, for the National Aeronautics and Space Administration under Contract NASW-3281, "Manufacturing in Space: Fluid Dynamics Numerical Analysis." The contractual effort described in this document was performed during the year from September 1981 to September 1982. The NASA Technical Director for this contract is Dr. Robert F. Dressler, Manager, Advanced Technology Program, NASA Headquarters, Washington, DC.

ACKNOWLEDGMENT

The authors are pleased to acknowledge the contribution to this effort of the NASA Technical Director, Dr. Robert F. Dressler. His suggestions and guidance contributed substantially to the overall program.

PRECEDING PAGE BLANK NOT FILMED

CONTENTS

INTRODUCTION

The research program described in this annual report is a continuation of effort initiated in August 1979 to investigate natural convection in various materials processing experiment configurations under microgravity conditions simulating the orbiting space station environment. The investigation involves the use of the Lockheed developed General Interpolants Method (GIM) fluid dynamics computer code to numerically simulate the development of natural convection under various loads.

Two basic tasks were performed during this year's effort:

1. Last year's investigation of the effects of changing the magnitude and direction of the acceleration vector was extended to include additional acceleration change sequences.
2. An investigation was made of the effect of enclosure shape on natural convection velocities.

The results of these tasks were published as separate documents which are included as Parts 1 and 2 of this annual report.

Part 1

NATURAL CONVECTION IN CIRCULAR ENCLOSURES FOR VARIOUS ORIENTATION'S OF THE ACCELERATION VECTOR

ABSTRACT

Numerical computations were performed for natural convection in circular enclosures under various conditions of acceleration. It was found that subcritical acceleration vectors applied in the direction of the temperature gradient will lead to an eventual state of rest regardless of the initial state of motion. Supercritical acceleration vectors will lead to the same steady state condition of motion regardless of the initial state of motion. Convection velocities were computed for acceleration vectors at various angles to the initial temperature gradient. The results for Rayleigh numbers of 1000 or less were found to closely follow Weinbaum's first order theory. Higher Rayleigh number results were shown to depart significantly from the first order theory. Supercritical behavior was confirmed for Rayleigh numbers greater than the known supercritical value of 9216. Response times were determined to provide an indication of the time required to change states of motion for the various cases considered.

PRECEDING PAGE BLANK NOT FILMED

CONTENTS

NOMENCLATURE

Symbol	Description
d	cylinder diameter = 2 R
g	gravity force
g_H	horizontal g component
g_V	vertical g component
r	radial distance
R	cylinder radius
Ra	Rayleigh number = $\frac{g\beta\ \Delta T\ d^3}{\nu\alpha}$
Ra_H	horizontal Rayleigh number
Ra_V	vertical Rayleigh number
T	temperature
T_o	initial mid-point temperature
ΔT	temperture difference across circular cylinder
t	time
t^*	response time
v	velocity
v_{max}	spatial maximum velocity
v_{max_o}	v_{max} for zero horizontal gravity component
Δv_{max}	$v_{max} - v_{max_o}$
x, y	rectangular coordinates (Fig. 1)

NOMENCLATURE (Concluded)

Symbol	Description
α	thermal diffusivity
β	volumetric coefficient of thermal expansion
Θ	polar angle (Fig. 1)
μ	dynamic viscosity
ν	kinematic viscosity, μ/ρ
ψ	stream function
ρ	density
ρ_o	ρ at $T = T_o$

INTRODUCTION

The investigation reported herein is basically a continuation of a previous investigation reported in Ref. 1. In the previous study, we investigated natural convection in circular enclosures in which the acceleration vector changes magnitudes and directions according to various schemes. The interest in the effect of time-varying acceleration loads on natural convection is due to current interest in space processing experiments in which small time-varying spacecraft accelerations in orbit will produce convective stirring in contained fluids. The previous study considered a circular enclosure with the acceleration load consisting of two components, a vertical component, g_V, applied normal to the initial temperature gradient and a horizontal component, g_H, in either the positive or negative direction parallel to the initial temperature gradient. The separate components were applied in the following sequences: (1) the vertical component applied until steady state, followed by the horizontal component superimposed to produce a new steady state; (2) both components applied simultaneously until steady state; and (3) the horizontal component applied first followed by the vertical component. This previous investigation showed that, for subcritical Rayleigh numbers, the imposition of a given set of vertical and horizontal components yields the same steady state convective flow field regardless of the order in which the two components are applied. The current study extends the preceding study to include the following conditions: (1) the vertical component applied until steady state, followed by removal of the vertical component and application of a horizontal component, and (2) application of a constant magnitude acceleration vector at various angles to the vertical direction.

As in the preceding study, the Lockheed-developed General Interpolants Method (GIM) code was used in the numerical computations. The computations were performed on the NASA-Langley CYBER 203 system.

ORIGINAL PAGE IS
OF POOR QUALITY

PROBLEM FORMULATION AND NUMERICAL SIMULATION

The problem investigated is that of two-dimensional natural convection within the circular cylinder enclosure shown in Fig. 1.

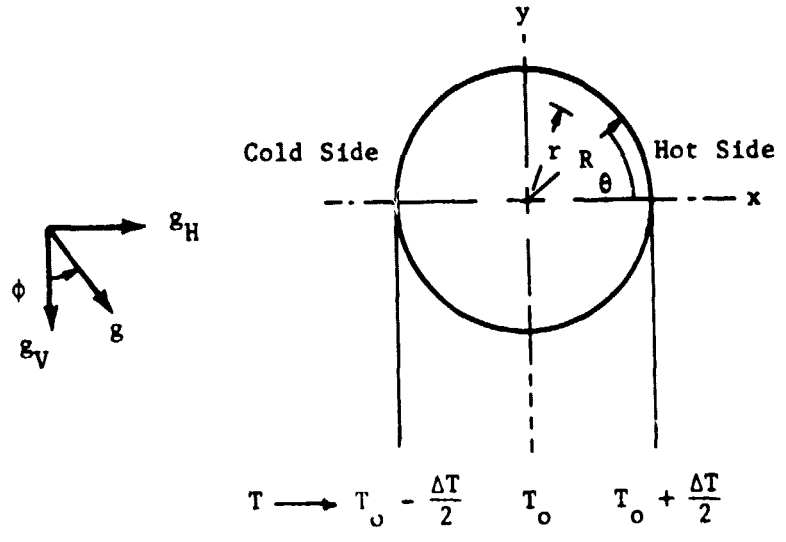

Fig. 1 - Geometry for Circular Cylinder Enclosure

The initial temperature distribution was based on a linear horizontal gradient in the positive x direction, with the boundary points held constant in time:

$$T(r,o) = T_o + (\Delta T/2)\, x/R$$

$$T(R,t) = T_o + (\Delta T/2) \cos\theta$$

The gravitation loading consisted of two components, a vertical component g_V in the negative y direction and a horizontal component in either the positive or negative x direction.

The numerical simulation was based on a nodal point distribution generated by the GIM code geometry module by specifying an array of 20 x 20 area elements with 21 x 21 nodal points. The circle was treated as a four-sided figure, each side being a quarter-circle arc. The circular area was divided into generalized quadrilateral elements with curvilinear sides, with the nodal points located at the four corners of each element. The circular geometry is shown in Fig. 2 with the computational grid network superimposed.

For convenience in the numerical simulation, we assumed a cylinder radius R of 1 cm and a temperature difference ΔT of 100 C. The gravity components were changed accordingly to yield the proper Rayleigh number values. The fluid was assumed to have the thermophysical properties of water and to behave as a Boussinesq fluid in its thermal expansion characteristics. The thermophysical properties used in the numerical simulation are listed as follows:

Property	Value
Viscosity, μ	1 centipoise
Thermal conductivity, k	0.00143 cal/cm-sec-C
Density, ρ	1 gm/cu cm
Specific heat, C_p	1 cal/gm-C
Thermal expansion coefficient, β	2.07×10^{-4}/C

ORIGINAL PAGE IS
OF POOR QUALITY

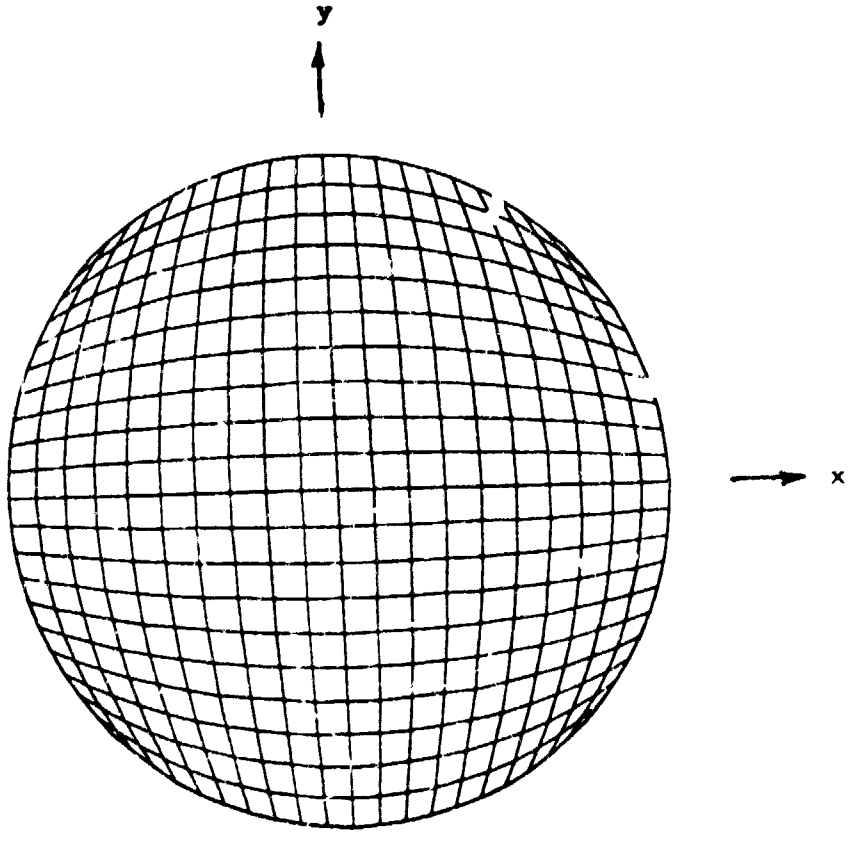

Fig. 2 - Geometry and Computatonal Grid for Numerical Simulation

RESULTS

Computed results are shown in Figs. 3 and 4 for the cases in which a vertical acceleration is applied until steady state followed by removal of the vertical acceleration and application of horizontal accelerations of various magnitudes in both the positive and negative x directions (see Fig. 1). Vertical Rayleigh numbers of 1000 and 5000 were considered, and their results are shown in Figs. 3 and 4, respectively. As indicated earlier in Ref. 2, a vertical Rayleigh number of 1000 is within the low Rayleigh number range for agreement with the first order theoretical results of Weinbaum (Ref. 3), while a vertical Rayleigh number of 5000 is somewhat out of that range. Horizontal accelerations corresponding to horizontal Rayleigh numbers of $\pm$1000, $\pm$2000, $\pm$5000 and $\pm$10,000 were considered. Results for the positive horizontal Rayleigh number of 10,000 are not shown on Figs. 3 and 4 because of its supercritical nature, as will be discussed later. Note in both Figs. 3 and 4 that the negative horizontal Rayleigh numbers result in a slowing down of the initial counterclockwise circulating flow, leading to a reversal in flow direction and followed by a continuous approach to a state of rest. The positive horizontal Rayleigh numbers, however, result in a continual decrease in flow velocity approaching zero without a flow reversal. A simplified analytical model described in the appendix basically confirms the validity of these trends.

Decay response times were calculated for the results in Figs. 3 and 4 to provide a quantitative indication of the time required for the flow to decay down to a state of rest after removal of the vertical acceleration and imposition of the horizontal acceleration. For the positive Ra_H values, the decay time is defined as the time required for the spatial maximum velocity to reach the fraction 1/e (.368) of the initial value. Because of the flow reversal that takes place for negative Ra_H values, the decay time for these cases is defined as the time required after passing through the minimum (maximum negative value) to reach the fraction 1/e of the minimum

ORIGINAL PAGE IS
OF POOR QUALITY

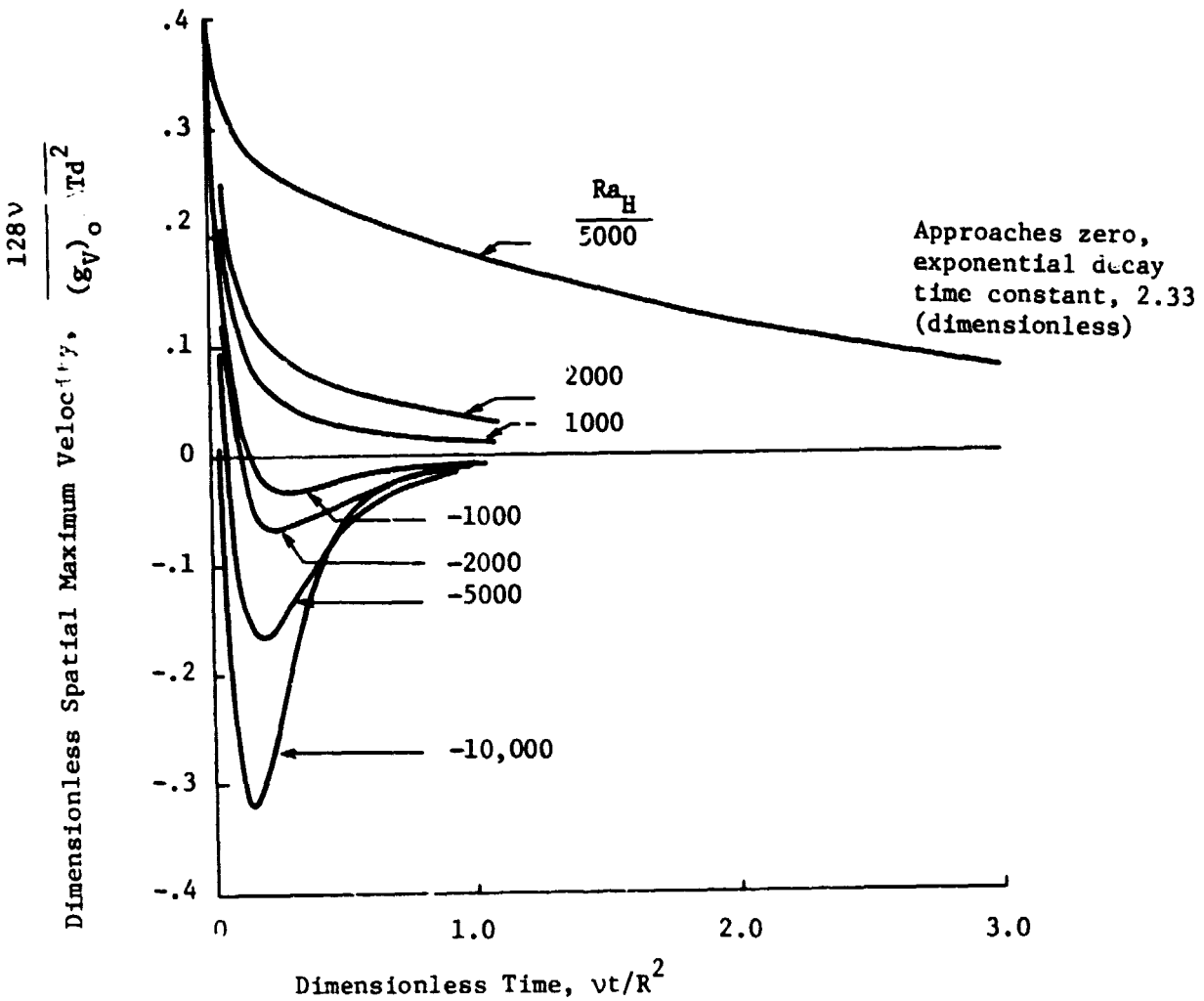

Fig. 3 - Spatial Maximum Velocity Histories After a Vertical Rayleigh Acceleration of 1000 is Removed and Various Horizontal Accelerations are Applied.

ORIGINAL PAGE IS
OF POOR QUALITY

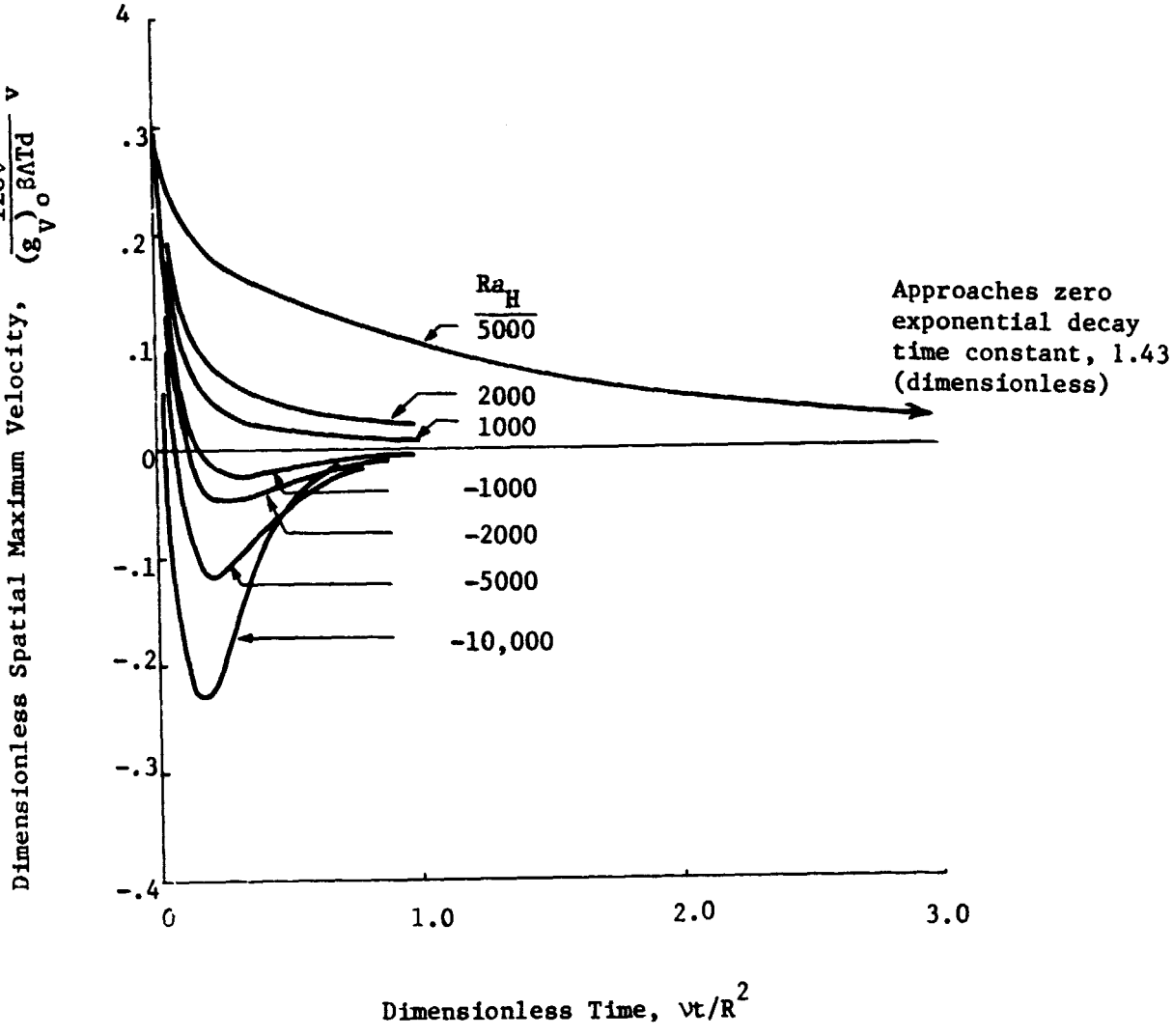

Fig. 4 - Spatial Maximum Velocity Histories After a Vertical Rayleigh Acceleration of 5000 is Removed and Various Horizontal Accelerations Are Applied

value. The decay times for initial vertical Rayleigh numbers of 1000 and 5000 are shown in Fig. 5. Note that the decay times for both Rayleigh numbers are essentially identical except in the range near a horizontal Rayleigh number of 5000. Decay times for negative Rayleigh numbers range from approximately 0.25 to 0.45 R^2/ν, and for positive Rayleigh numbers from approximately 0.1 to 1.6 R^2/ν. According to Weinbaum's theory, in the absence of a vertical acceleration component and for horizontal Rayleigh numbers less than the critical value of 9216, any velocity perturbation will be damped out, and convective motion will not develop. This critical value also follows from the simplified analysis in the appendix. In horizontal Rayleigh numbers greater than the critical value, however, a small perturbation in velocity will grow, and convective motion will develop. Shown in Fig. 6 is a comparison of convective motion resulting from a supercritical positive horizontal Rayleigh number of 10,000 applied to various initial states of motion. The initial states resulted from vertical Rayleigh numbers of 0, 1000 and 5000 applied until steady state and then removed. (It was necessary to initialize the fluid flow with a small perturbaton for the zero vertical Rayleigh number case for convective motion to develop.) Note that regardless of the initial state of motion, the convective motion proceeds toward the same steady state condition. In each case, an overshoot in the spatial maximum velocity occurs, followed by a continual decrease to the steady state value.

A comparison is made in Fig. 7 of convective motion resulting from the two supercritical horizontal Rayleigh numbers of 10,000 and 20,000. A vertical Rayleigh number of 5000 was used to initialize the state of motion in both cases. The 10,000 horizontal Rayleigh number case is the same as that shown in Fig. 6. The 10,000 Rayleigh number case shows an initial increase and subsequent continued decay to steady state. The 20,000 Rayleigh number case displays a strongly oscillating, although damped, approach to a steady state spatial maximum velocity approximately twice the 10,000 Rayleigh number case. These limited results suggest a proportional relationship between horizontal acceleration and the resulting spatial

ORIGINAL PAGE IS
OF POOR QUALITY

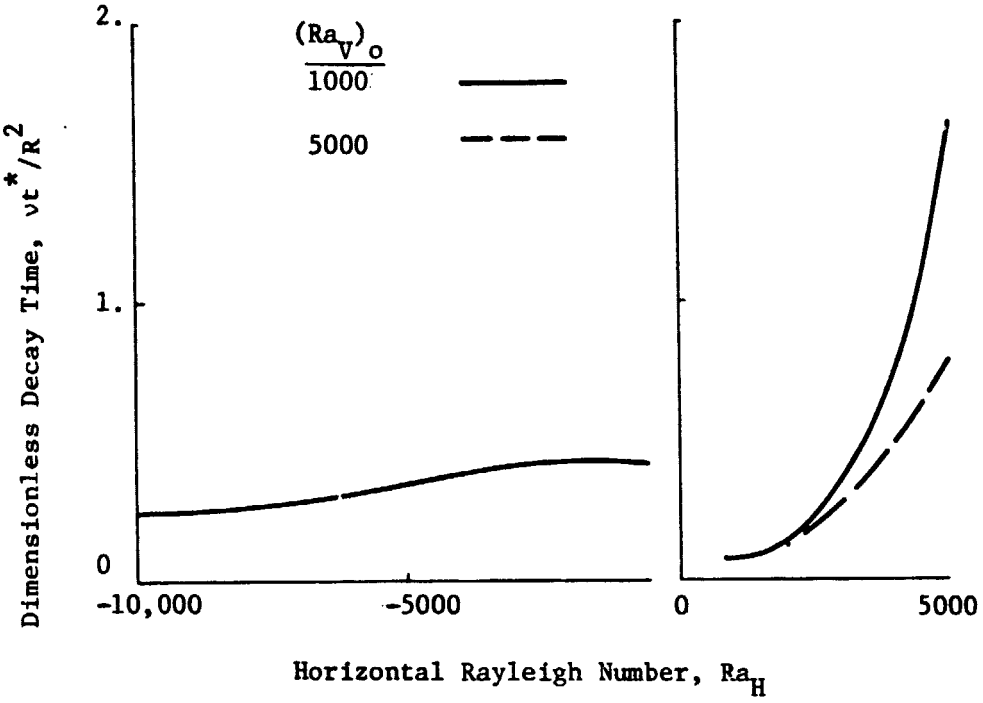

Fig. 5 - Decay Time for Flow Initialized by Vertical Acceleration, Followed by Removal of Vertical Acceleration and Imposition of Horizontal Acceleration

ORIGINAL PAGE IS
OF POOR QUALITY

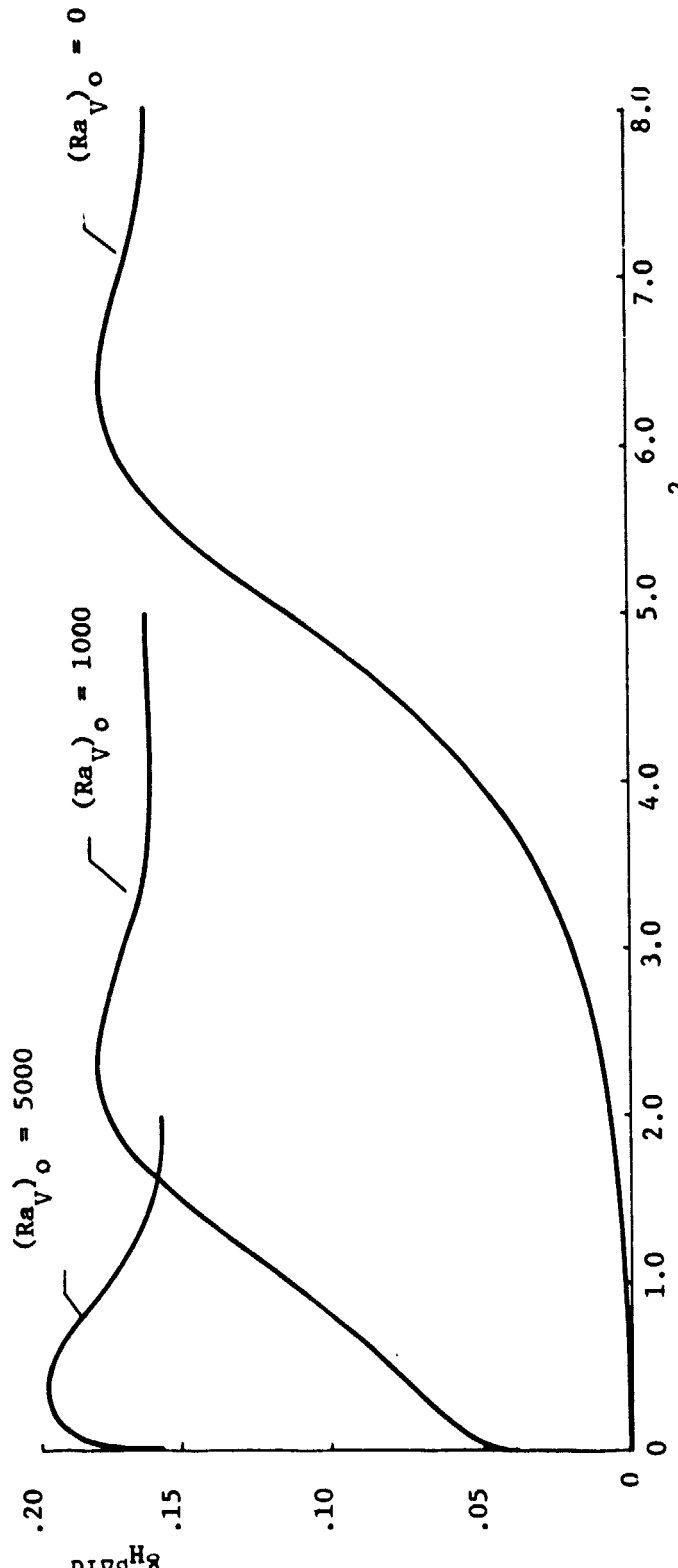

Fig. 6 - Comparison of Spatial Maximum Velocity Histories After Various Initial Vertical Rayleigh Accelerations are Removed and Horizontal Supercritical Acceleration (Ra_H = 10,000) is Applied

ORIGINAL PAGE IS
OF POOR QUALITY

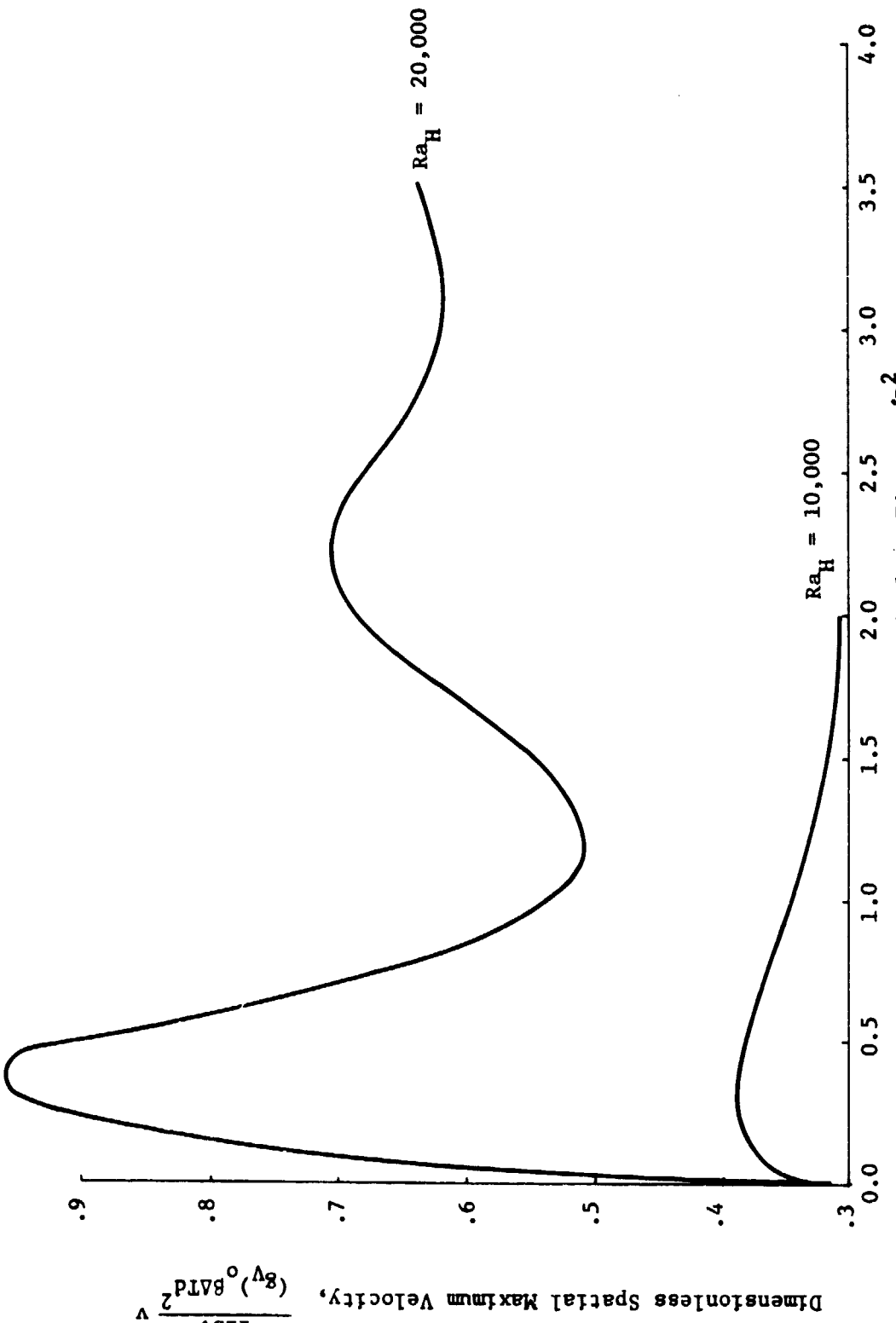

Fig. 7 - Comparison of Spatial Maximum Velocity Histories After a Vertical Rayleigh Acceleration of 5000 is Removed and Supercritical Horizontal Accelerations Ra_H = 10,000 and 20,000 are Applied

maximum convective velocities for supercritical cases. Such a relationship would certainly break down near the critical Rayleigh number, however, since the steady state velocity goes to zero for Rayleigh numbers less than the critical value.

The results shown in Figs. 8-10 are for acceleration vectors of constant magnitude applied at various angles to the vertical direction. The magnitudes of the acceleration vectors correspond to Rayleigh numbers of 1000, 5000 and 10,000.

The steady state results are compared in Fig. 11 to the low Rayleigh number (first order) theory of Weinbaum which considers only the vertical component. The Ra = 1000 results are very nearly identical to Weinbaum's theory, thus indicating "low Rayleigh number" conditions. The Ra = 5000 results show considerable skewness in the curve, indicating deviation from low Rayleigh conditions, but still goes to zero at ϕ = 90 deg, indicating subcritical conditions. The Ra = 10,000 results are clearly out of the low Rayleigh number range, and indicate supercritical conditions, since non-zero steady state velocities occur at ϕ = 90 deg.

Transient response times were calculated for the results in Figs. 8, 9 and 10 to provide an indication of the time required for development of convective flow. Since some of the results showed an overshoot in velocity followed by decay to steady state, the response time was defined as the time required to reach the fraction 1-1/e (.632) of the maximum velocity acheived either at steady state or during the overshoot prior to steady state, whichever is greater. The resulting response times are shown in Fig. 12 as a function of the horizontal Rayleigh number component for the various absolute Rayleigh number values. The simplified analytical development outlined in the appendix indicates that response times should be horizontal Rayleigh number dependent. The results shown in Fig. 12 indicate a general variation in response time from approximately 0.05 R^2/ν for negative horizontal Rayleigh numbers to approximately 0.20 R^2/ν for positive horizontal Rayleigh numbers. Note that, except for some scatter in the 5000 Rayleigh

ORIGINAL PAGE IS
OF POOR QUALITY

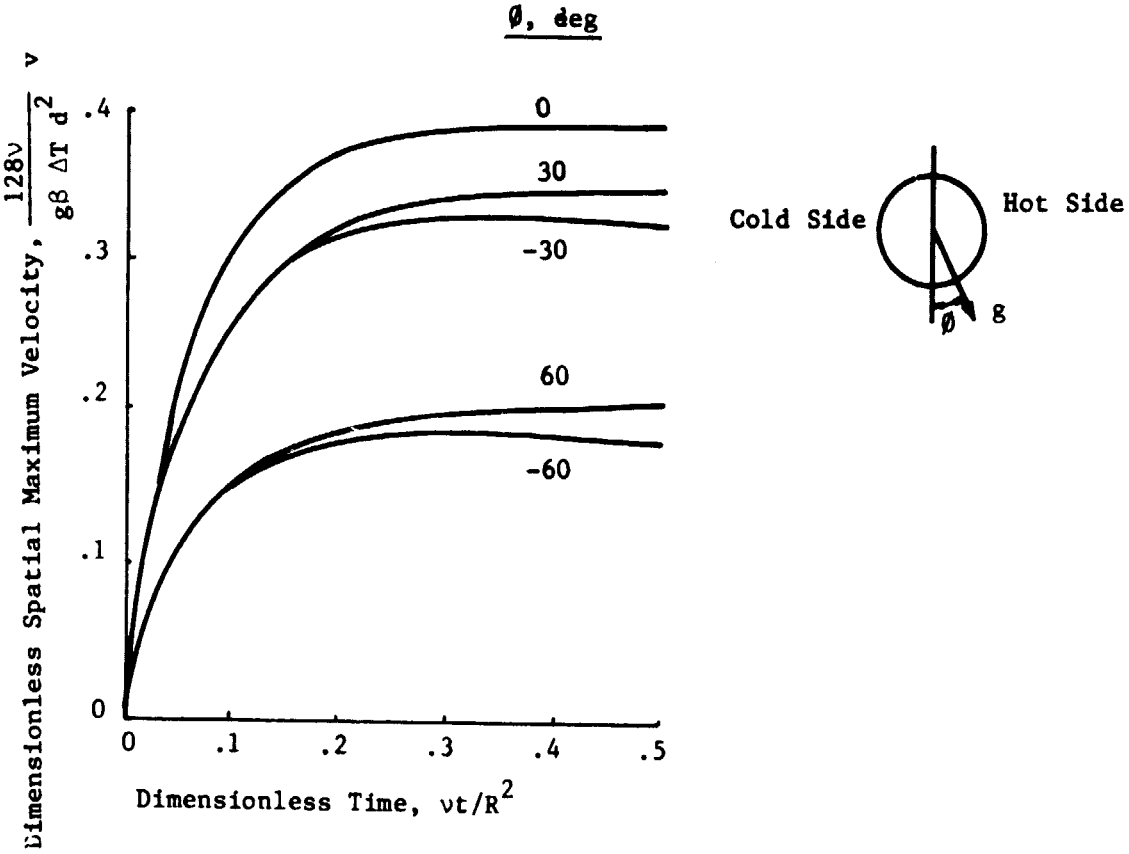

Fig. 8 - Spatial Maximum Velocity History Starting from Rest for Ra = 1000 and Various Off-Vertical Angles

ORIGINAL PAGE IS
OF POOR QUALITY

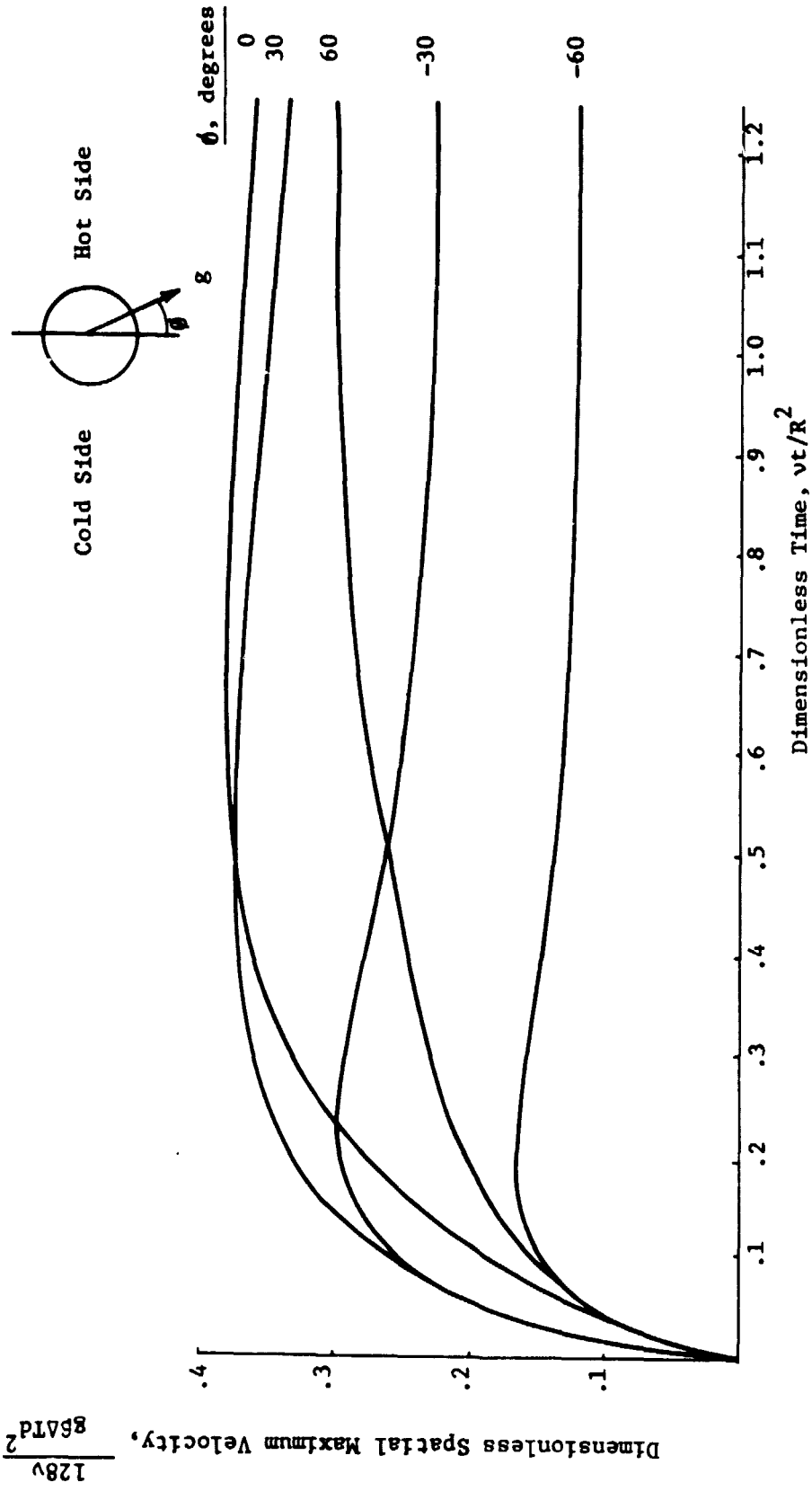

Fig. 9 - Spatial Maximum Velocity History Starting from Rest for Ra = 5,000 and Various Off-Vertical Angles

ORIGINAL PAGE IS
OF POOR QUALITY

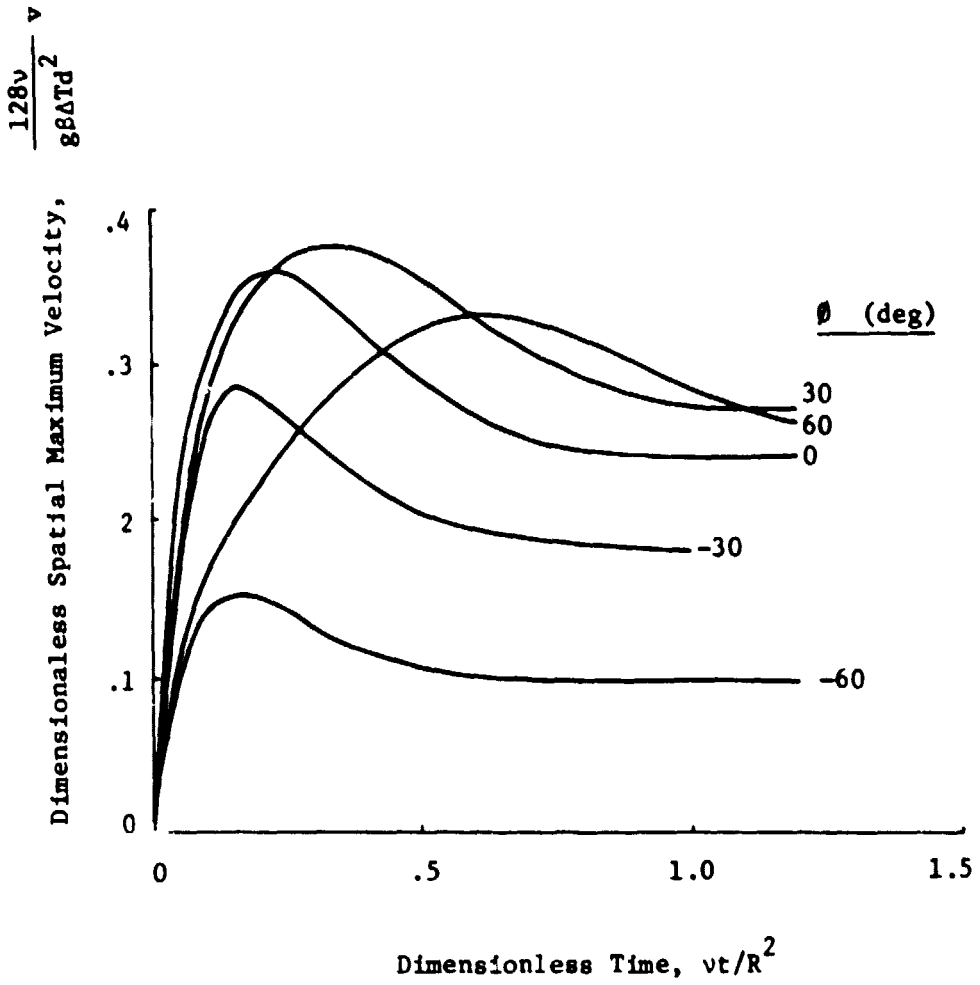

Fig. 10 - Spatial Maximum Velocity History Starting from Rest for Ra = 10,000 and Various Off-Vertical Angles

ORIGINAL PAGE IS
OF POOR QUALITY

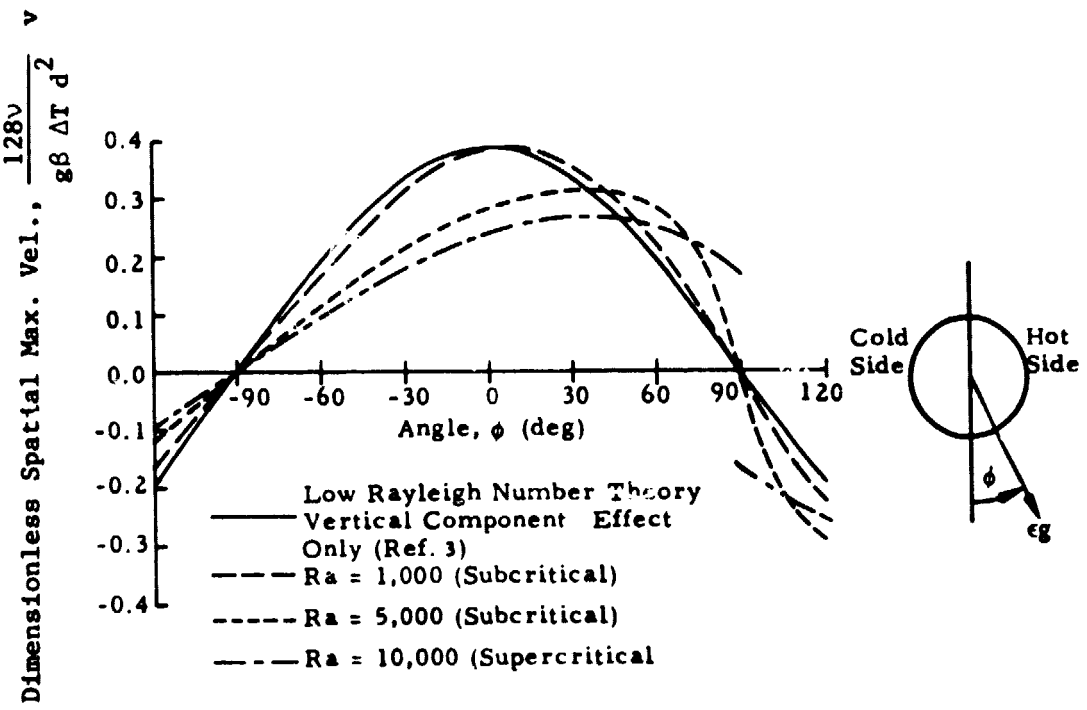

Fig. 11 - Variation of Steady State Spatial Maximum Velocity with Angle Varying Between Vertical and Horizontal

ORIGINAL PAGE IS
OF POOR QUALITY

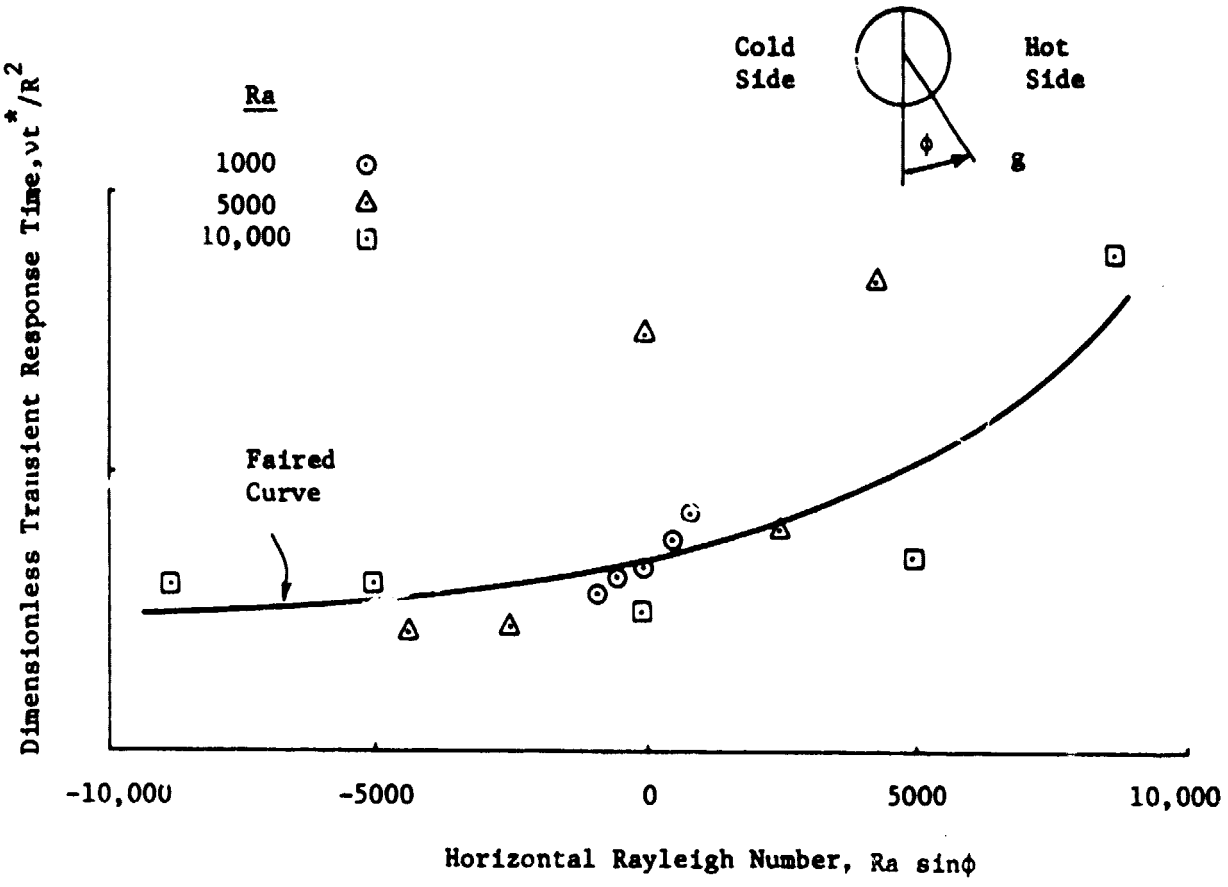

Fig. 12 - Transient Response Times versus Horizontal Rayleigh Number for Various Absolute Rayleigh Numbers

number data, the results over the range of Rayleigh numbers considered closely follow a general trend indicated by the faired curve.

Contour plots of temperature, absolute velocity and stream function are shown in Figs. 13 through 16 for the case of a 1 cm radius circular enclosure containing water with a temperature difference of 100 K across the horizontal diameter. The acceleration vector was varied to correspond to the noted Rayleigh number values.

The temperature contours at steady state are presented in Fig. 13 for a vertical Rayleigh number of 1000 and horizontal Rayleigh numbers of 0, $\pm$1000 and $\pm$5000. The positive horizontal components are shown to noticeably increase the distortion in the isotherms as expected. The negative horizontal components decrease the distortion somewhat, but not as noticeably as in the positive case.

The velocity contours at steady state are shown in Fig. 14, again for a vertical Rayleigh number of 1000 and horizontal Rayleigh numbers of 0, $\pm$1000 and $\pm$5000. The exhibited flow appears to be nearly perfectly circular in all cases with the maximum velocity indicated roughly near the r = 0.5 to 0.6 radial position. The theoretical maximum occurs at $r = R/\sqrt{3} = 0.58$ R. Some of the departure from circular symmetry in the velocity contours is probably due to the numerical noise in computing such small velocities. The circularity of the flow is more clearly indicated by the streamline contours shown in Fig. 15. A nearly perfectly circular flow pattern is shown in all cases.

The development of convective flow from rest for the supercritical Ra_H = 10,000 case is illustrated by the contour plots of temperature and streamlines in Fig. 16. Steady state was reached in this case without break up into multiple convective cells because of the low value of Ra_H.

ORIGINAL PAGE IS
OF POOR QUALITY

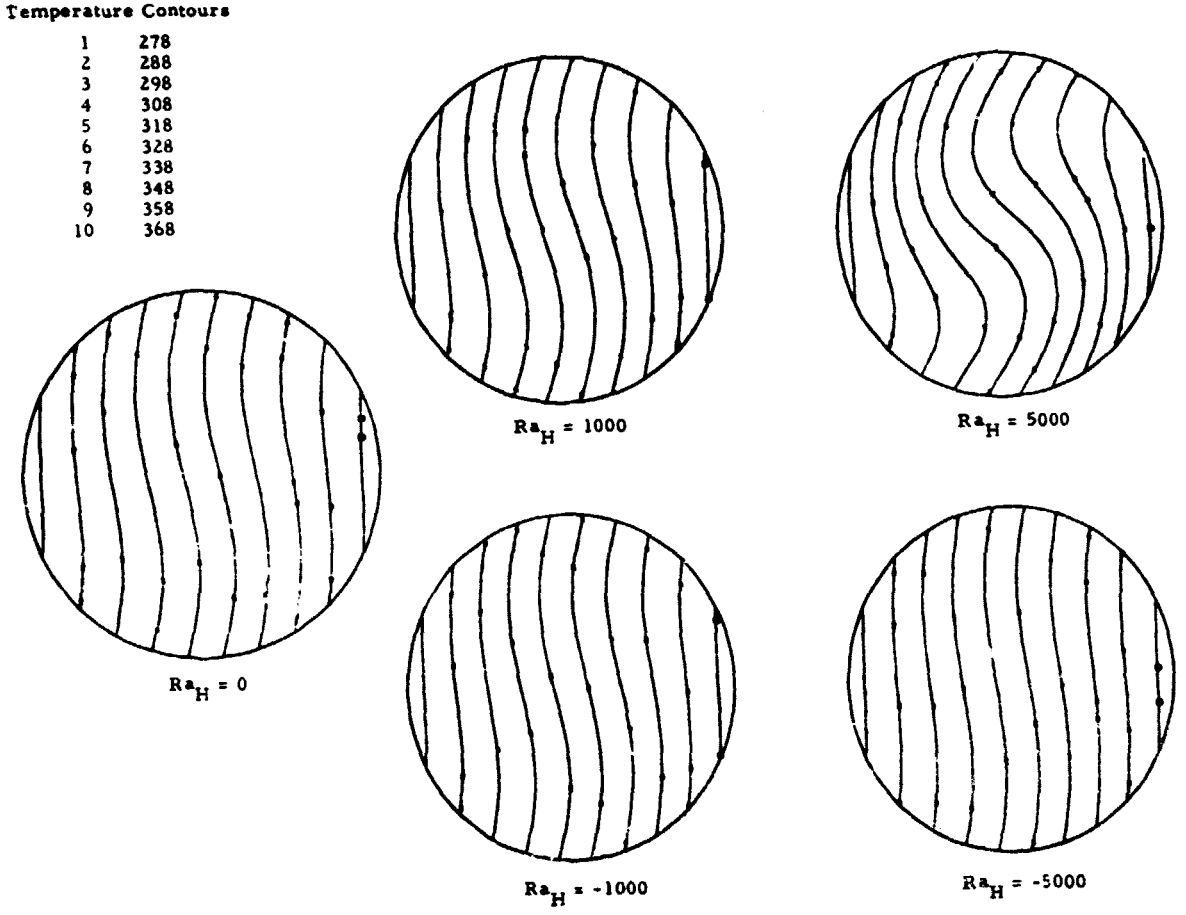

Fig. 13 - Temperature Contours at Steady State for Various Horizontal Rayleigh Numbers (Ra_V = 1000, Temperature Units = K)

ORIGINAL PAGE IS
OF POOR QUALITY

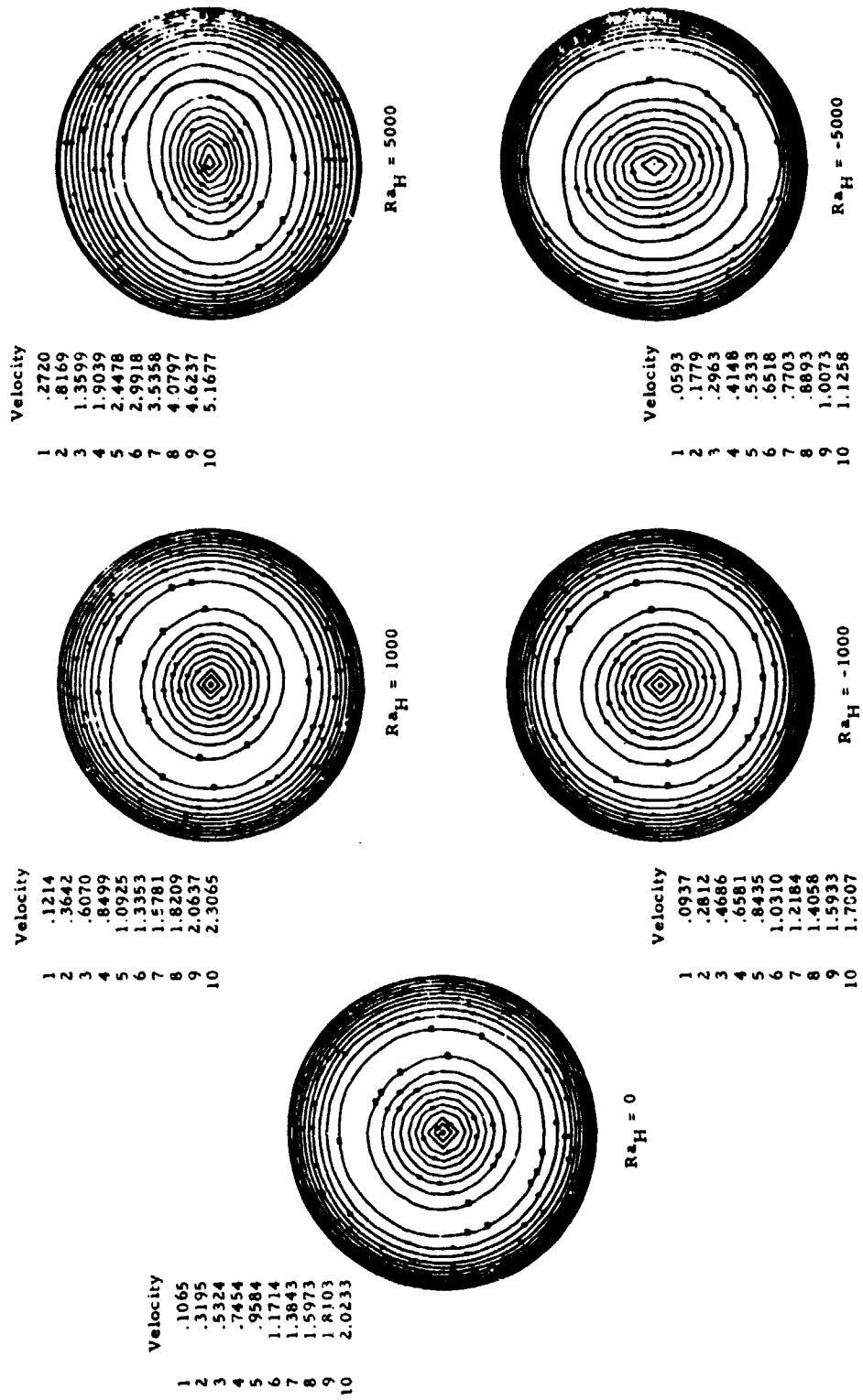

Fig. 14 - Velocity Contours at Steady State for Various Horizontal Rayleigh Numbers (Ra_V = 1000, Velocity Units = 10^{-3} cm/sec)

ORIGINAL PAGE IS
OF POOR QUALITY

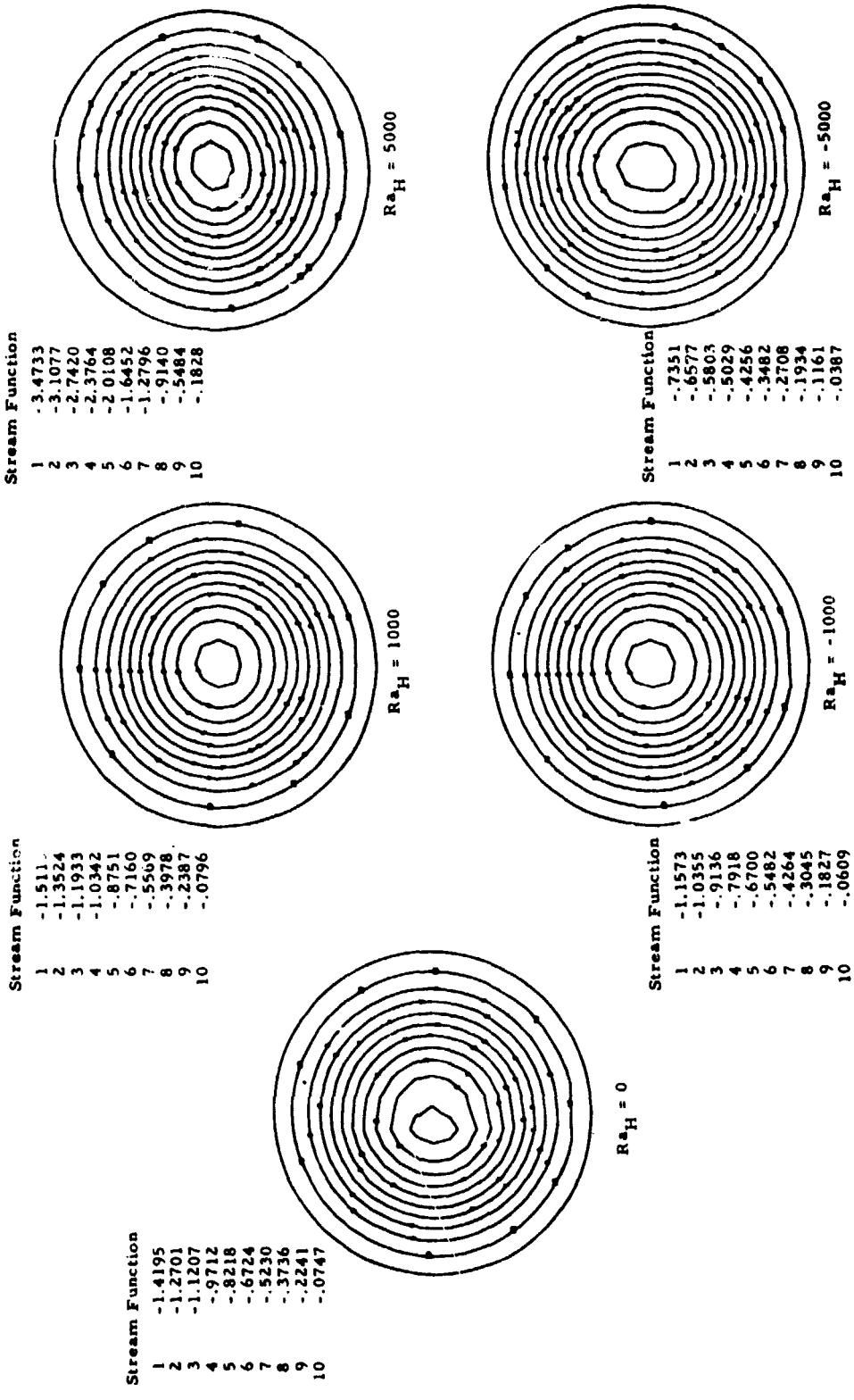

Fig. 15 - Streamlines at Steady State for Various Horizontal Rayleigh Numbers (Ra_V = 1000, Stream Function Units = 10^{-3} cm^2/sec)

ORIGINAL PAGE IS
OF POOR QUALITY

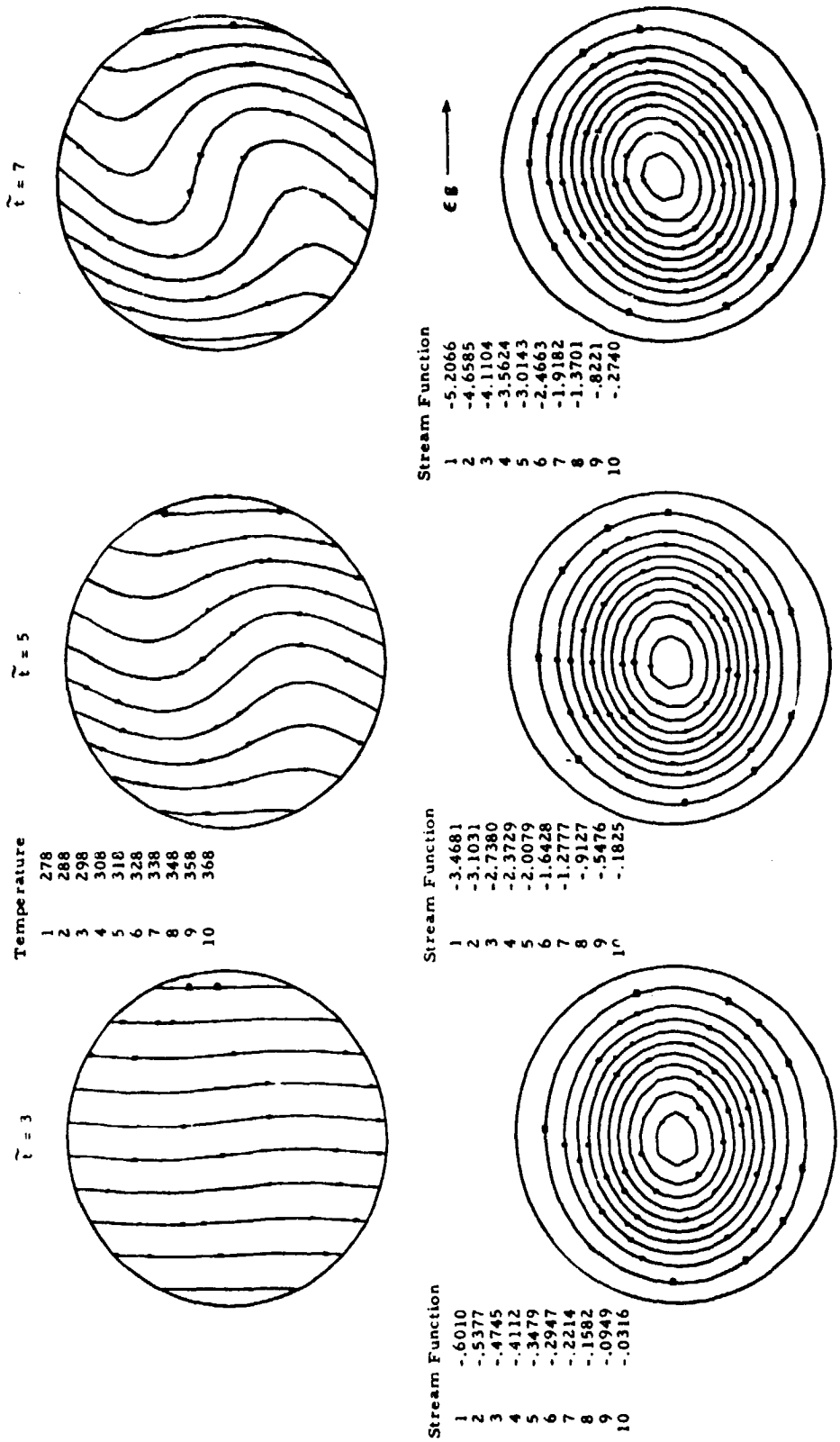

Fig. 16 - Temperature Contours and Streamlines at Various Times for Ra_H = 10,000
(Ra_V = 0, Temperature Units = K, Stream Function Units = 10^{-3} cm^2/sec)

CONCLUSIONS

The following general conclusions may be drawn from this study:

1. Subcritical accelerations applied in the direction of the initial temperature gradient will result in an eventual return to a state of rest, regardless of the intensity of the initial state of motion.

2. Supercritical accelerations applied in the direction of the initial temperature gradient will result in an approach to the same steady state convective motion regardless of the initial state of motion.

3. The variation in steady state velocities with angle at which the acceleration vector is applied closely follows Weinbaum's first order theory for absolute Rayleigh numbers of 1000 or less. For Rayleigh numbers greater than 1000, the deviation from Weinbaum's theory becomes significant.

REFERENCES

1. Robertson, S. J., and L. W. Spradley, "Numerical Simulation of Natural Convection with Gravity-Shift in Circular Cylinders in Low Gravity," LMSC-HREC TR D784161, Lockheed Missiles & Space Company, Inc., Huntsville, Ala., March 1981.

2. Robertson, S. J., L. W. Spradley, and M. P. Goldstein, "Numerical Analysis of Natural Convection in Two-Dimensional Square and Circular Containers in Low Gravity," LMSC-HREC TR D697821, Lockheed Missiles & Space Company, Inc., Huntsville, Ala., August 1980.

3. Weinbaum, S., "Natural Convection in a Horizontal Circular Cylinder," J. Fluid Mech., Vol. 18, 1964, p. 409.

4. Dressler, R. F., NASA Headquarters, Washington, D. C. (to be published).

ORIGINAL PAGE IS
OF POOR QUALITY

Appendix

SIMPLIFIED ANALYTICAL MODEL FOR NATURAL CONVECTION IN A HORIZONTAL TWO-DIMENSIONAL CIRCULAR ENCLOSURE

A simplified analytical model was developed to predict natural convection in two-dimensional circular enclosures. The purpose of the simplified model is to provide a basis for verifying the GIM code numerical results, and to assist in defining time constants for the computed transient response. The model development is similar to that reported in Ref. A-1. The geometry is indicated in Fig. A-1.

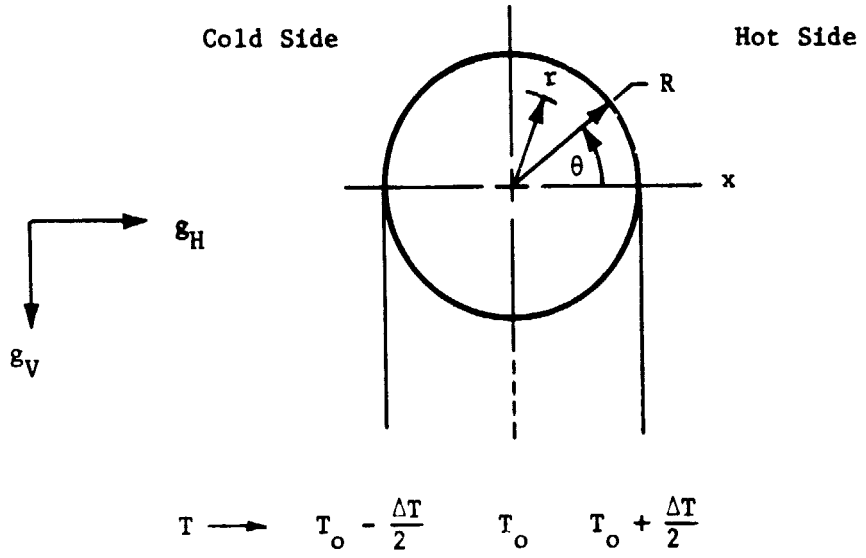

Fig. A-1 - Geometry for Circular Cylinder Enclosure

The initial temperature distribution was based on a linear horizontal gradient in the positive x direction, with the boundary points held constant in time:

$$T(r,o) = T_o + (\Delta T/2)\ x/R$$
$$T(R,t) = T_o + (\Delta T/2)\ \cos\theta \qquad (1)$$

We assume the usual circular flow pattern with the velocity profile given by

$$v = \frac{3\sqrt{3}}{2}\ v_{max}\ [1 - (r/R)^2]\ (r/R) \qquad (2)$$

with v_{max} varying with time during the transient flow period. We take the counter clockwise direction as positive, since the convective flow will assume this direction for a positive vertical acceleration component.

We also assume the transient temperature distribution given by

$$T = T_o + \frac{\Delta T}{2}\ (r/R)\ \cos\theta + T' \qquad (3)$$

where T' is a perturbation term due to convective flow given by

$$T' = \frac{3\sqrt{3}}{2}\ T'_{max}\ [1 - (r/R)^2]\ (r/R)\ \sin\theta \qquad (4)$$

with T'_{max} varying with time. Along the y axis ($\theta = \pi/2$), the perturbed temperature distribution follows the same form as the velocity distribution given by Eq.2.

ORIGINAL PAGE IS
OF POOR QUALITY

The fluid density distribution is based on a Boussinesq variation with temperature:

$$\rho = \rho_o \left[1 - \beta (T - T_o)\right] \tag{5}$$

The torque, M_V, on the fluid mass due to viscous shear stress on the interior cylinder surface is given by

$$\begin{aligned} M_V &= 2\pi R\mu \left.\frac{\partial v}{\partial r}\right|_{r = R} \\ &= - 6\pi \sqrt{3}\, \mu\, v_{max}\, R \end{aligned} \tag{6}$$

The torque due to gravity M_G is found by:

$$M_G = - \iint \rho(g_V\, x + g_H\, y)\, dS \tag{7}$$

where the integration is carried out over the circular region. The vertical gravity component g_V is always positive and acts in the negative y direction. The horizontal component, g_H, may be either positive or negative according to its direction with respect to the x axis. Carrying out the integration of Eq.(7) yields

$$M_G = - \int_0^{2\pi} \int_0^{R} \rho(g_V \cos\theta + g_H \sin\theta)\, r^2\, dr\, d\theta \tag{8}$$

$$= \frac{\pi}{8} \rho_o \beta \Delta T\, R^3\, (g_V + \sqrt{3}\ T'_{max}\, g_H)$$

ORIGINAL PAGE IS
OF POOR QUALITY

The instantaneous angular momentum of the fluid mass is given by:

$$P = \iint r\, \rho v\, dS \tag{9}$$

where, again, the integration is carried out over the circular region. Carrying out this integration yields

$$P = \int_0^{2\pi} \int_0^{R} \rho\, v r^2\, dr\, d\theta$$

$$= \frac{\sqrt{3}}{4}\, \pi R^3\, \rho_o\, v_{max} \tag{10}$$

By balancing the rate of change of angular momentum to the net torque on the fluid mass, a differential equation is obtained for the variation of v_{max} with time:

$$dP/dt = M_G + M_V$$

$$\frac{\sqrt{3}}{4}\, \pi R^3\, \rho_o\, \dot{v}_{max} = \frac{\pi}{8}\, \rho_o \beta \Delta T\, R^3 \left(g_V + \sqrt{3}\, T'_{max}\, g_H \right) - 6\pi\, \sqrt{3}\, \mu R\, v_{max} \tag{11}$$

or

$$\dot{v}_{max} = \frac{1}{16\sqrt{3}}\, \frac{\alpha \nu}{R^3} \left(Ra_V + \sqrt{3}\, \frac{T'_{max}}{\Delta T}\, Ra_H \right) - 24\, \frac{\nu}{R^2}\, v_{max} \tag{12}$$

This differential equation contains two dependent variables, v_{max} and T'_{max}. A second equation is thus required for a solution. We used the unsteady conduction equation,

ORIGINAL PAGE IS
OF POOR QUALITY

$$\frac{\partial T}{\partial t} + \vec{v} \cdot \nabla T = \alpha \nabla^2 T \tag{13}$$

evaluated at the point of maximum velocity and temperature perturbation along the y axis, $r = 1/\sqrt{3}$ ($x = 0$, $y = 1/\sqrt{3}$), for the required second equation. Finding the temperature gradient and Laplacian at $x = 0$ and $y = 1/\sqrt{3}$ from Eqs.(3) and (4) and solving Eq.(13) yields:

$$\dot{T}'_{max} = \frac{\Delta T}{2R} v_{max} - 12 \frac{\alpha}{R^2} T'_{max} \tag{14}$$

A single differential equation in terms of v_{max} is obtained by differentiating Eq.(12) and combining with Eq.(14):

$$\ddot{\tilde{v}}_{max} + 12 \frac{2\,Pr + 1}{Pr} \dot{\tilde{v}}_{max} + \frac{288}{Pr} \left(1 - \frac{Ra_H}{9216}\right) \tilde{v}_{max} - \frac{3}{4\sqrt{3}} \frac{Ra_V}{Pr^2} = 0 \tag{15}$$

where the tilda denotes normalization of the velocity to the characteristic velocity, ν/R; time to the characteristic time, R^2/ν; and temperature to the temperature difference, ΔT. The general solution of Eq.(15) is

$$\tilde{v}_{max} = C_1 e^{m_1 \tilde{t}} + C_2 e^{m_2 \tilde{t}} + \frac{1}{384\sqrt{3}} \frac{Ra_V}{Pr \left(1 - \frac{Ra_H}{9216}\right)} \tag{16}$$

where

$$m_1 = -6 \frac{(2\,Pr + 1)}{Pr} \left[1 - \sqrt{1 - 8 \frac{Pr}{(2\,Pr + 1)^2} \left(1 - \frac{Ra_H}{9216}\right)}\right] \tag{17}$$

$$m_2 = -6 \frac{(2\,Pr + 1)}{Pr} \left[1 + \sqrt{1 - 8 \frac{Pr}{(2\,Pr + 1)^2} \left(1 - \frac{Ra_H}{9216}\right)}\right] \tag{18}$$

ORIGINAL PAGE IS
OF POOR QUALITY

$$C_1 = \left\{ 6 \frac{(2\,Pr + 1)}{Pr} \left[1 + \sqrt{1 - 8 \frac{Pr}{(2\,Pr+1)^2} \left(1 - \frac{Ra_H}{9216}\right)} \right] \left[(\tilde{v}_{max})_0 - \frac{1}{384\sqrt{3}} \frac{Ra_V}{Pr\left(1 - \frac{Ra_H}{9216}\right)} \right] \right.$$

$$\left. - \frac{Ra_V}{16\sqrt{3}\,Pr} - \frac{Ra_H}{16} (\tilde{T}'_{max})_0 + 24\,\tilde{v}_{max})_0 \right\} \div$$

$$\left\{ 12 \frac{(2\,Pr + 1)}{Pr} \sqrt{1 - 8 \frac{Pr}{(2\,Pr + 1)^2} \left(1 - \frac{Ra_H}{9216}\right)} \right\} \qquad (19)$$

$$C_2 = -\left\{ 6 \frac{(2\,Pr + 1)}{Pr} \left[1 - \sqrt{1 - 8 \frac{Pr}{(2\,Pr + 1)^2} \left(1 - \frac{Ra_H}{9216}\right)} \right] \left[(\tilde{v}_{max})_0 - \frac{1}{384\sqrt{3}} \frac{Ra_V}{Pr\left(1 - \frac{Ra_H}{9216}\right)} \right] \right.$$

$$\left. + \frac{Ra_V}{16\sqrt{3}\,Pr} + \frac{Ra_H}{16} (\tilde{T}'_{max})_0 - 24\,(\tilde{v}_{max})_0 \right\} \div$$

$$\left\{ 12 \frac{(2\,Pr + 1)}{Pr} \sqrt{1 - 8 \frac{Pr}{(2\,Pr + 1)^2} \left(1 - \frac{Ra_H}{9216}\right)} \right\} \qquad (20)$$

where the zero subscripts denote initial conditions.

We are particularly concerned with the following sequence. First a vertically downward gravity force is imposed until a steady state condition is reached. The vertical gravity force is then removed, and a horizontal gravity force is imposed until a new steady state condition is reached. Considering the instant of imposition of the horizontal force as the starting time, the initial conditions are as follows:

ORIGINAL PAGE IS
OF POOR QUALITY

$$(\tilde{v}_{max})_0 = \frac{(Ra_V)_0}{384\sqrt{3}\ Pr} \tag{21}$$

$$(\tilde{T}'_{max})_0 = \frac{(Ra_V)_0}{9216\sqrt{3}} \tag{22}$$

where $(Ra_V)_0$ is the Rayleigh number corresponding to the initially imposed vertical gravity force.

For this case, Eq.16 becomes:

$$\tilde{v}_{max} = (\tilde{v}_{max})_0 \Bigg\{ 1 + \frac{(2\ Pr+1)\left[1 - \sqrt{1 - 8\frac{Pr}{(2\ Pr+1)^2}\left(1 - \frac{Ra_H}{9216}\right)}\right] - 4\ Pr\left(1 - \frac{Ra_H}{9216}\right)}{2(2\ Pr+1)\sqrt{1 - 8\frac{Pr}{(2\ Pr+1)^2}\left(1 - \frac{Ra_H}{9216}\right)}} \Bigg\}$$

$$\exp\left\{-6\frac{2Pr+1}{Pr}\left[1 - \sqrt{1 - 8\frac{Pr}{(2\ Pr+1)^2}\left(1 - \frac{Ra_H}{9216}\right)}\right]\tilde{t}\right\}$$

$$- \frac{(2\ Pr+1)\left[1 - \sqrt{1 - 8\frac{Pr}{(2\ Pr+1)^2}\left(1 - \frac{Ra_H}{9216}\right)}\right] - 4\ Pr\left(1 - \frac{Ra_H}{9216}\right)}{2(2\ Pr+1)\sqrt{1 - 8\frac{Pr}{(2\ Pr+1)^2}\left(1 - \frac{Ra_H}{9216}\right)}}$$

$$\exp\left\{-6\frac{2\ Pr+1}{Pr}\left[1 + \sqrt{1 - 8\frac{Pr}{(2\ Pr+1)^2}\left(1 - \frac{Ra_H}{9216}\right)}\right]\tilde{t}\right\} \Bigg\} \tag{23}$$

ORIGINAL PAGE IS
OF POOR QUALITY

For Pr = 7 (water), Eq.(23) reduces to the following double exponential equations for the noted Ra_H values.

- $Ra_H = -5000$

$$\tilde{v}_{max}/(\tilde{v}_{max})_0 = (-\ 0.694\ e^{-2.76\ \tilde{t}} + 1.69\ e^{-22.96\ \tilde{t}}) \qquad (24)$$

- $Ra_H = +5000$

$$\tilde{v}_{max}/(\tilde{v}_{max})_0 = (0.577\ e^{-0.772\ \tilde{t}} + 0.423\ e^{-24.95\ \tilde{t}}) \qquad (25)$$

These equations are shown plotted in Fig. A-2 compared with GIM code numerically computed results for initial vertical Rayleigh number, $(Ra_V)_0$, values of 1000 and 5000. Note that the analytical curves predict a flow reversal prior to an eventual decay to a state of rest for the negative horizontal Rayleigh number cases ($Ra_H = -5000$). The GIM code results show good agreement with the analytical results for $Ra_H = -5000$ for both the 1000 and 5000 $(Ra_V)_0$ values. Good agreement is also shown for the $(Ra_V)_0 = 5000$, $(Ra_V) = +5000$ case. $(Ra_V)_0 = 1000$, $Ra_H = +5000$ case does not exhibit the same degree of agreement as the other cases, but the exponential decay trend is roughly the same for both the analytical and numerical results.

ORIGINAL PAGE IS
OF POOR QUALITY

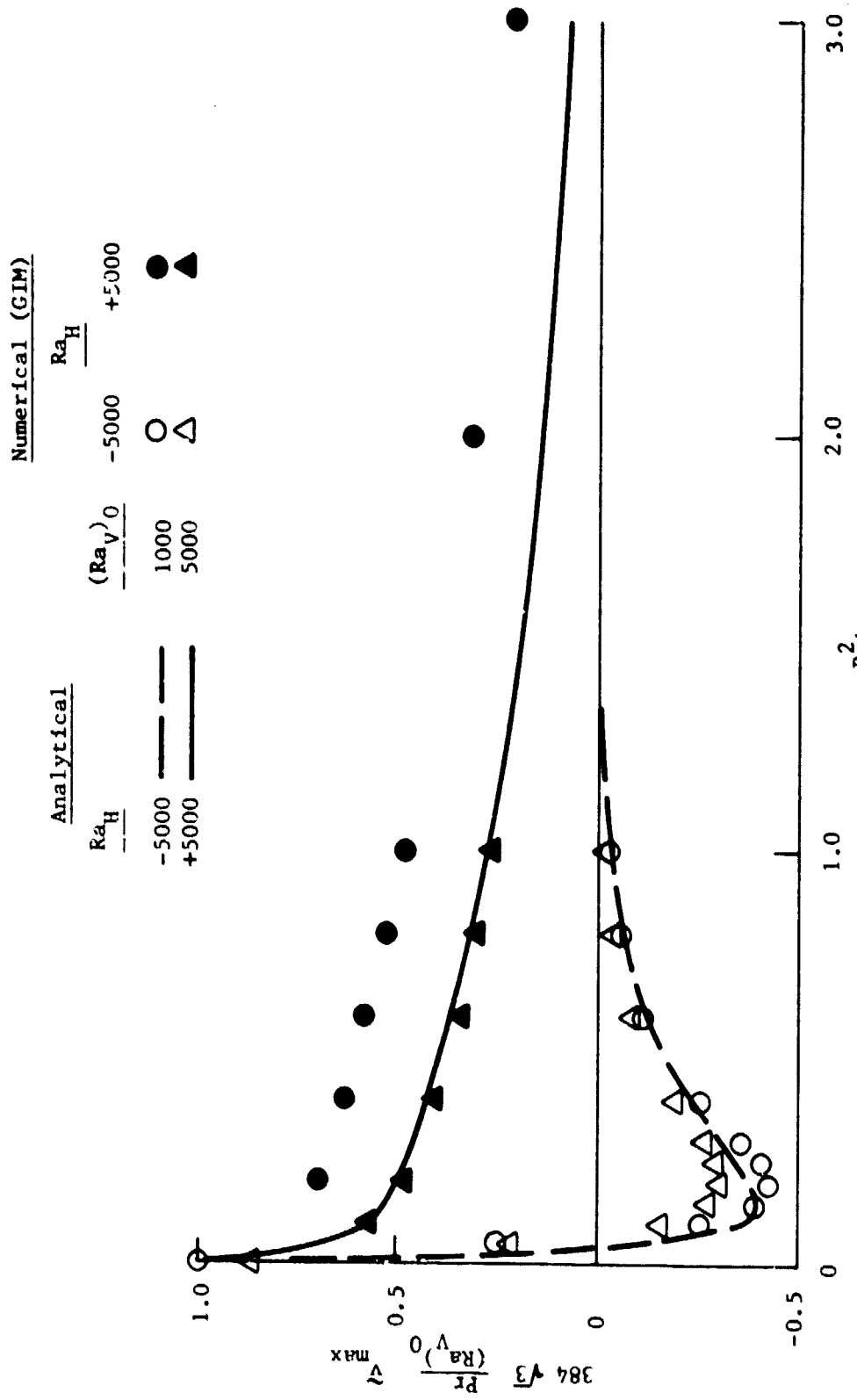

Fig. A-2 - Comparison of GIM Code Numerical Results to Simplified Analytical Model for Gravity-Shift Cases

Part 2

EFFECT OF ENCLOSURE SHAPE ON NATURAL CONVECTION VELOCITIES

REDSTONE ARSENAL RESEARCH & ENGINEERING CENTER

ABSTRACT

A numerical analysis was performed to compare natural convection velocities in two-dimensional enclosures of various shape. The following shapes were investigated: circle, square, horizontal and upright 2 x 1 aspect ratio rectangles, horizontal and upright half-circles, diamond (square oriented with diagonal vertical) and triangle (equilateral with horizontal base). In all cases, the length scale in the various dimensionless parameters, such as Rayleigh number, is defined as the diameter of the equal area circle. Natural convection velocities were calculated for Rayleigh numbers of 1000 and 5000 with the temperature difference taken to be across (a) the maximum horizontal dimension, (b) the median horizontal line (line through centroid) and (c) the horizontal distance such that the temperature gradient is the same for shapes of equal area. A Rayleigh number of 1000 is within the "low Rayleigh number" range for agreement with first order theory for circular enclosures. A Rayleigh number of 5000 is slightly out of this range. For the class of shapes including the square, upright half-circle and upright rectangle, the computed velocities were found to agree very closely with that of the equal area circle when the temperature difference is taken to be across the maximum horizontal dimension (condition (a)). The velocities for the horizontal rectangle and half circle were found to be approximately one-half that of the equal area circle for the same condition. Better overall agreement among all shapes was obtained by setting the temperature difference across a distance such that the temperature gradients were equal for shapes of equal area.

PRECEDING PAGE BLANK NOT FILMED

CONTENTS

PRECEDING PAGE BLANK NOT FILMED

NOMENCLATURE

Symbol	Description
d	equal area circle diameter
g	gravity force
R	circle radius
Ra	Rayleigh number = $\frac{g\beta\Delta T d^3}{\nu\alpha}$
ΔT	temperature difference
t	time
v	velocity
α	thermal diffusivity
β	volumetric coefficient of thermal expansion
μ	dynamic viscosity
ν	kinematic viscosity, μ/ρ
ψ	stream function
ρ	density

PRECEDING PAGE BLANK NOT FILMED

1. INTRODUCTION

A number of fluid mechanics experiments are to be performed aboard orbiting spacecraft, primarily to investigate the possible use of the near-zero gravity environment in various materials processing applications. A knowledge of the intensity of convective stirring due to residual accelerations is required in order to properly plan and evaluate the experiments. Various shaped containers will be used in these experiments. Theoretical results have been obtained which yield exact predictions of natural convection velocities in an idealized container, i.e., the two-dimensional circular enclosure (Ref. 1). It would be helpful for estimation purposes if a reasonable means existed for the extrapolation of the circular enclosure results to more complex shapes. A previous study demonstrated extremely good agreement in computed natural convection velocities for circular and square enclosures of equal cross-sectional area (Ref. 2). Dressler (Ref. 3) made use of this noted agreement in circular and square enclosure results, in addition to the more general results documented herein, to analyze natural convection in the proposed Lal, Kroes and Wilcox crystal growth experiment to be performed infight on Spacelab 3. The purpose of this investigation is to develop reasonable extrapolation criteria by comparing numerically computed natural convection velocities for various two-dimensional enclosure shapes with the circular enclosure results. The Lockheed-developed General Interpolant Method (GIM) computer code (Ref. 4) was used in the numerical computations.

2. METHOD OF APPROACH AND NUMERICAL SIMULATION

The following set of two-dimensional enclosure shapes was considered: circle, square, 2 x 1 aspect ratio rectangle in both upright and horizontal orientations, half-circle in both upright and horizontal orientations, diamond (square oriented with diagonal vertical) and triangle (equilateral with horizontal base). The baseline condition was selected for equal area with the temperature difference set across the maximum horizontal dimension. The initial temperature distribution was based on a uniform horizontal gradient with the boundary points held constant in time. The gravity vector was considered to be constant in the downward direction. The fluid was assumed to behave as a boussinesq fluid in its thermal expansion characteristics.

The numerical simulation was based on dividing the various enclosures into a computational grid consisting of a network of generalized quadrilateral elements with curvilinear sides, with the nodal points located at the four corners of each element. Each of the enclosures considered in this study was treated as a generalized quadrilateral region divided by interpolation into an array of 20 x 20 elements. For example, the circle was treated as a four-sided figure, each side being a quarter-circle arc.

The triangle was treated by forming a parallelogram such that two adjacent sides and the diagonal formed the desired triangle. The entire parallelogram was divided into a computational grid, but the diagonal points were treated as boundary points. The parallelogram with the diagonal boundary thus formed two independent triangular regions. The computational grids for the enclosures considered in this study are shown in Figs. 1 - 5.

The grids for the square and diamond are the same since the diamond is simply a square with the diagonal in the upright position. The rectangle and half-circle grids are identical in either the upright or horizontal positions.

3. RESULTS

The velocity histories for the various shaped enclosures are shown in Figs. 6 and 7 for Rayleigh numbers of 1000 and 5000. The various enclosures are all of equal area, with the dimensionless velocities and Rayleigh numbers defined based on a temperature difference ΔT across the maximum horizontal dimension, and a length scale equal to the diameter d of the equal area circle. Note that, for a Rayleigh number of 1000 the steady state velocities of the equal area circle and square are very close to identical, with the upright rectangle and half-circle being within about 5% of the circle value. The horizontal rectangle and half-circle, and the triangle steady state velocities form another grouping of values approximately one-half the circle value. The diamond results appear approximately midway between the two extremes. Roughly the same trend of steady state values appear for a Rayleigh number of 5000. Overall, the steady state velocities for the various equal area enclosures are in agreement within a factor of approximately 2.

Response times for the various enclosure results are shown in Fig. 8 for both 1000 and 5000 Rayleigh number. Agreement within a factor of approximately 2 is shown for all enclosures. These response times are defined as the time required to reach the fraction 1 - 1/e (0.632) of the maximum or steady state velocities, whichever is greater, in Figs. 6 and 7.

An attempt was made to find other bases for correlating the data to yield better agreement between the results for the various shaped enclosures. Including the base line correlation, described earlier, correlations were made for the following sets of conditions concerning the distance over which the temperature difference was taken:

- Temperature difference across maximum horizontal dimension (base line correlation).

- Temperature difference across median horizontal line (line through centroid). Only the triangle and horizontal half-circle results changed in this correlation from the baseline correlation.

- Temperature difference taken across a distance such that the temperature gradient is the same for all shapes.

The steady state results for the above sets of correlations are summarized in Fig. 9 for a Rayleigh number of 1000, and in Fig. 10 for a Rayleigh number of 5000. For each of the correlation sets, the length scale in the Rayleigh number and dimensionless velocity is taken to be the diameter of the equal area circle. A comparison of the three correlation sets shows improved correlation for the triangle and horizontal half-circle by taking the temperature difference across the median horizontal line rather than the maximum horizontal dimension. Generally better correlation is obtained by setting the temperature gradients equal. This is equivalent to taking the temperature difference across a distance equal to the diameter of the equal area circle.

Computer generated streamline, absolute velocity and temperature contour plots for all of the enclosures are shown in Figs. 11 through 34 at steady state for both 1000 and 5000 Rayleigh numbers.

4. CONCLUSIONS

Natural convection velocities within two-dimensional enclosures of various shape, for Rayleigh numbers up to at least 5000, may be estimated with reasonable accuracy by considering the area to be equivalent to a circle of equal area. For the class of figures including the square, upright half-circle, and upright 2 x 1 aspect ratio rectangle, excellent agreement is obtained by considering the temperature difference across the maximum horizontal dimension to be equal to that across the equal area circle horizontal diameter. The agreement of the two upright oblong shapes indicates probable agreement for any similar upright oblong shape of roughly the same aspect ratio.

The horizontal oblong shapes have natural convection velocities approximately one-half that estimated based on the equal area circle with the temperature difference across the maximum horizontal dimension taken to be equal to that across the equal area circle diameter. As with the upright shapes, this probably indicates a general pattern for similar oblong shapes of roughly the same aspect ratio.

Better overall agreement among all shapes is obtained by setting the temperature difference across a distance equal to the diameter of the equal area circle, thus making the temperature gradients equal for any shape.

REFERENCES

1. Weinbaum, S., "Natural Convection in a Horizontal Circular Cylinder," J. Fluid Mech., Vol. 18, 1964, p. 409.

2. Robertson, S.J., L.W. Spradley and M.P. Goldstein, "Numerical Analysis of Natural Convection in Two-Dimensional Square and Circular Containers in Low Gravity," LMSC-HREC TR D697821, Lockheed Missiles & Space Company, Inc., Huntsville, Ala., August 1980.

3. Dressler, Robert F., "Approximate Analysis of Thermal Convection in a Crystal-Growth cell for Spacelab 3," NASA Technical Paper 2026, June 1982.

4. Spradley, L.W., and M.L. Pearson, "GIM Code User's Manual for the STAR-100 Computer," NASA Contractor Report 3157, November 1979.

ORIGINAL PAGE IS
OF POOR QUALITY

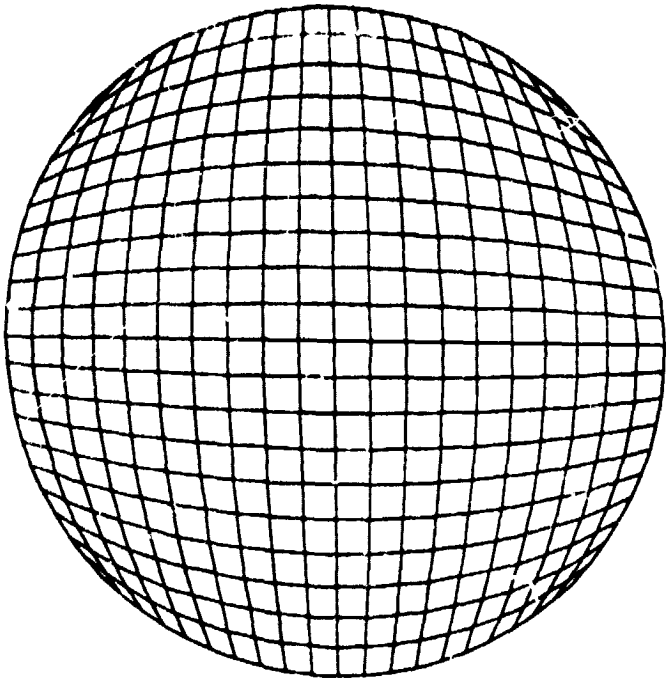

Fig. 1 - Computational Grid: Circle

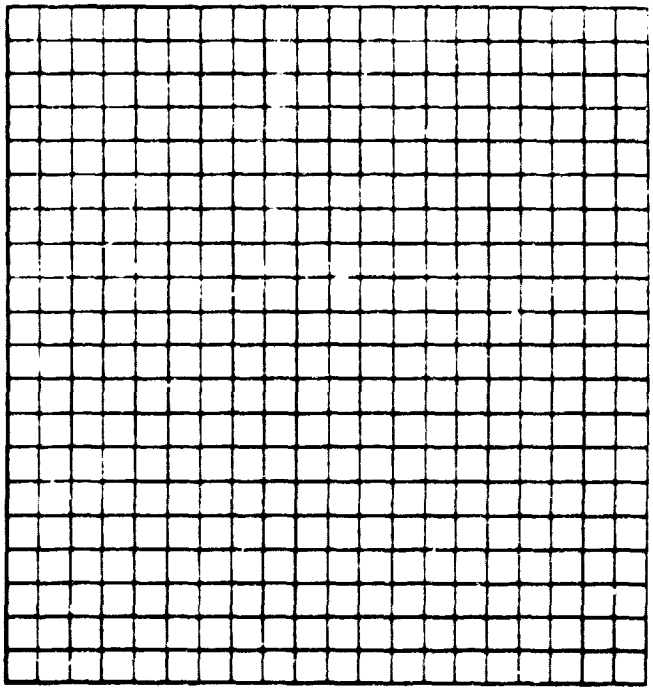

Fig. 2 - Computational Grid: Square and Diamond

ORIGINAL PAGE IS
OF POOR QUALITY

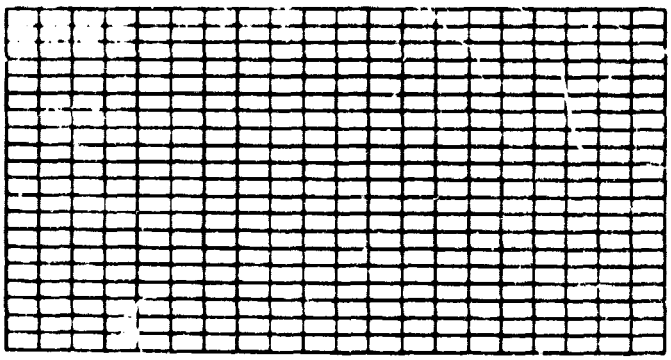

Fig. 3 - Computational Grid: 2x1 Aspect Ratio Rectangle

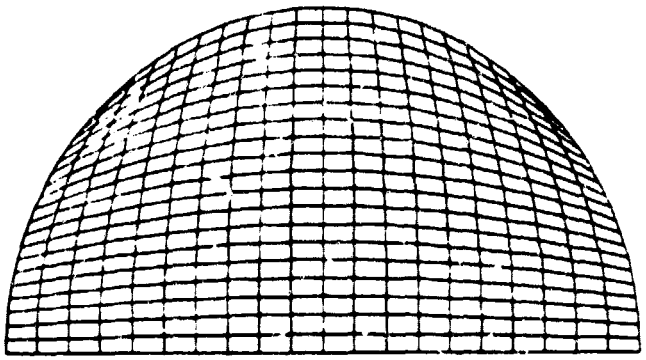

Fig. 4 - Computational Grid: Half-Circle

ORIGINAL PAGE IS
OF POOR QUALITY

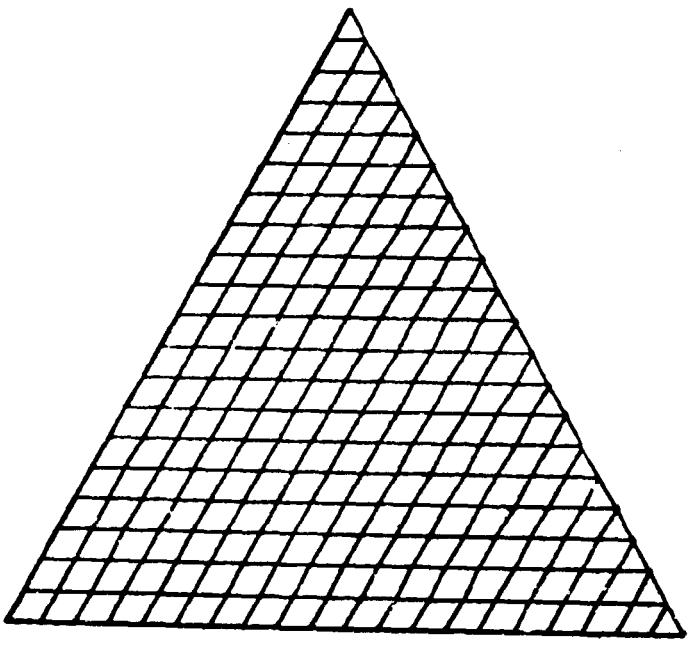

Fig. 5 - Computational Grid: Triangle

ORIGINAL PAGE IS
OF POOR QUALITY

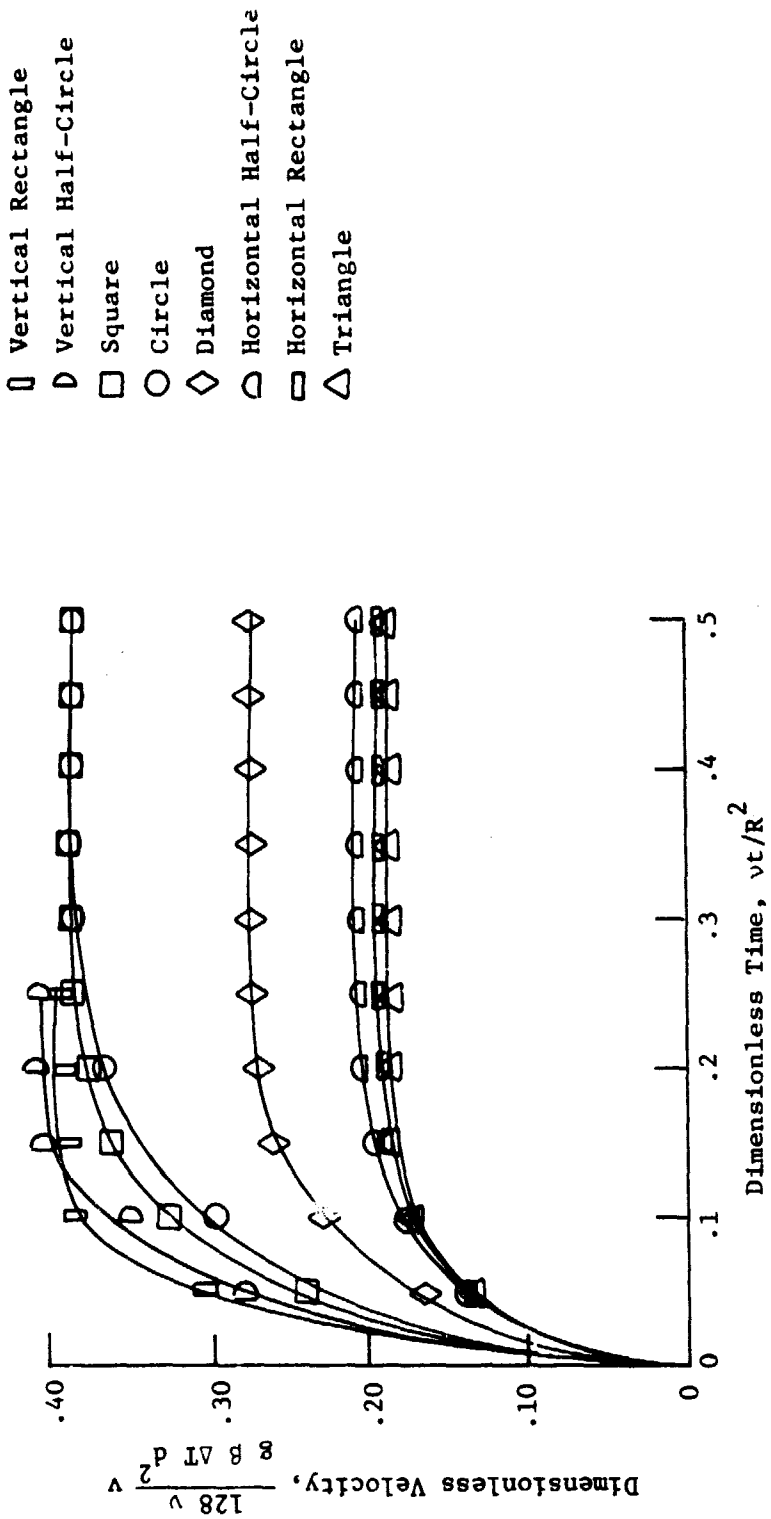

Fig. 6 - Velocity Histories for Natural Convection in Two-Dimensional Enclosures of Various Shape and Raleigh Number of 1000

ORIGINAL PAGE IS
OF POOR QUALITY

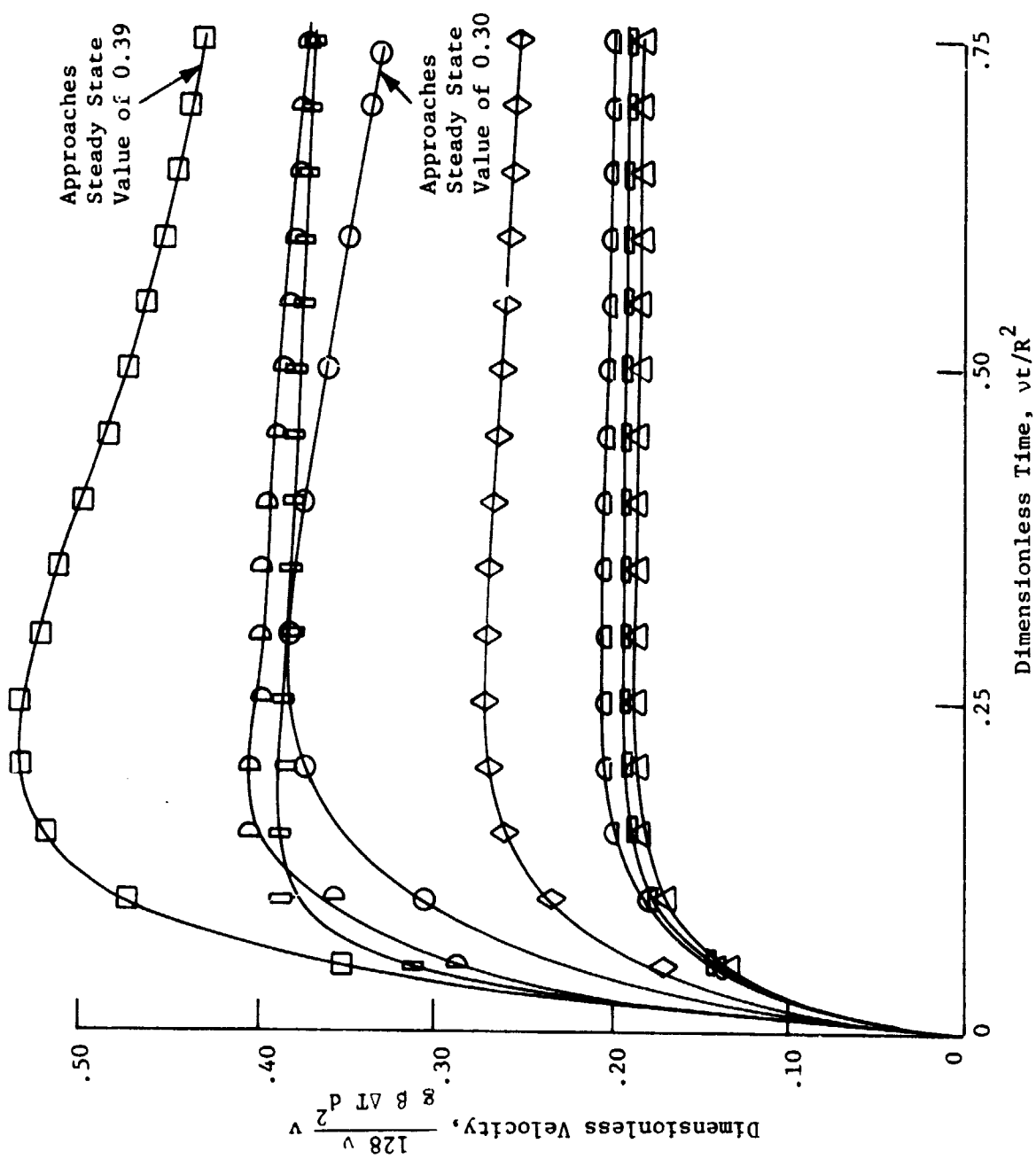

Fig. 7 - Velocity Histories for Natural Convection in Two-Dimensional Enclosures of Various Shape and Rayleigh Number of 5000

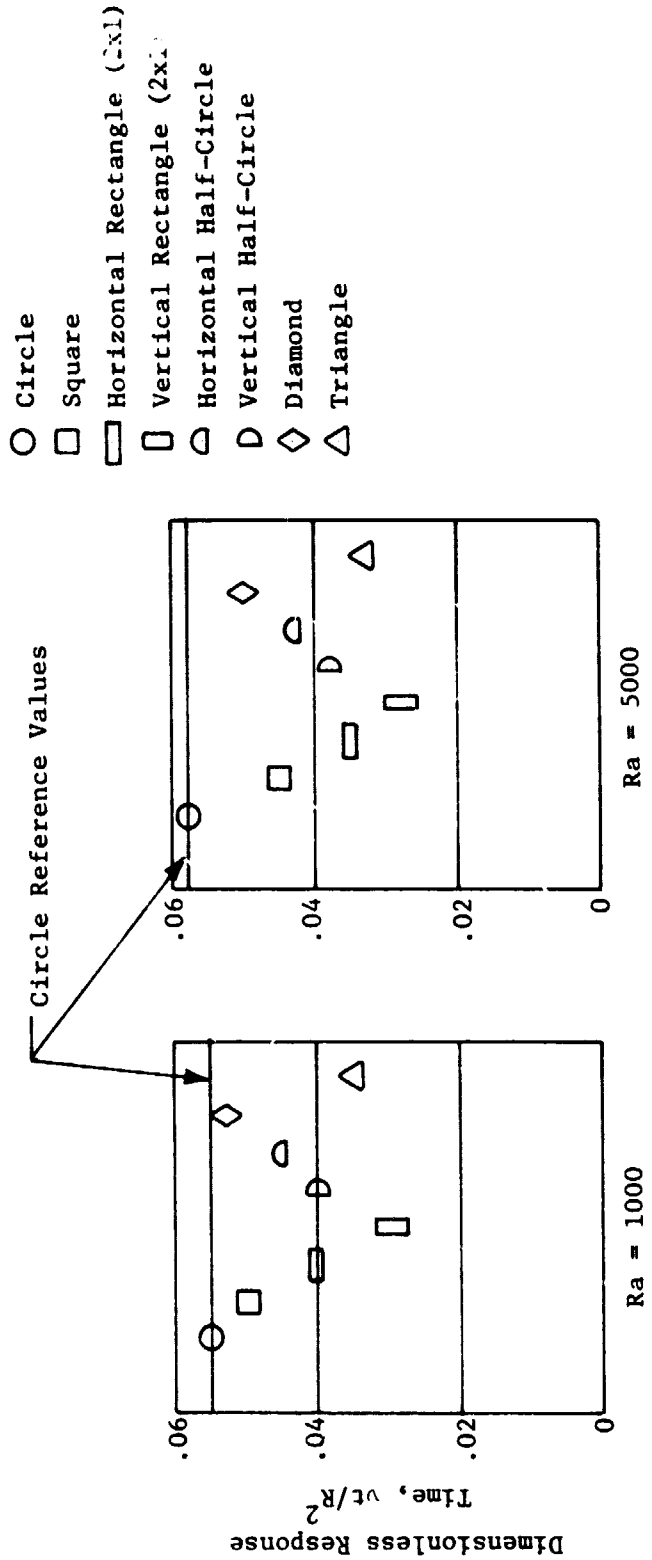

Fig. 8 - Comparison of Response Times for Natural Convection in Two-Dimensional Enclosures of Various Shape

ORIGINAL PAGE IS
OF POOR QUALITY

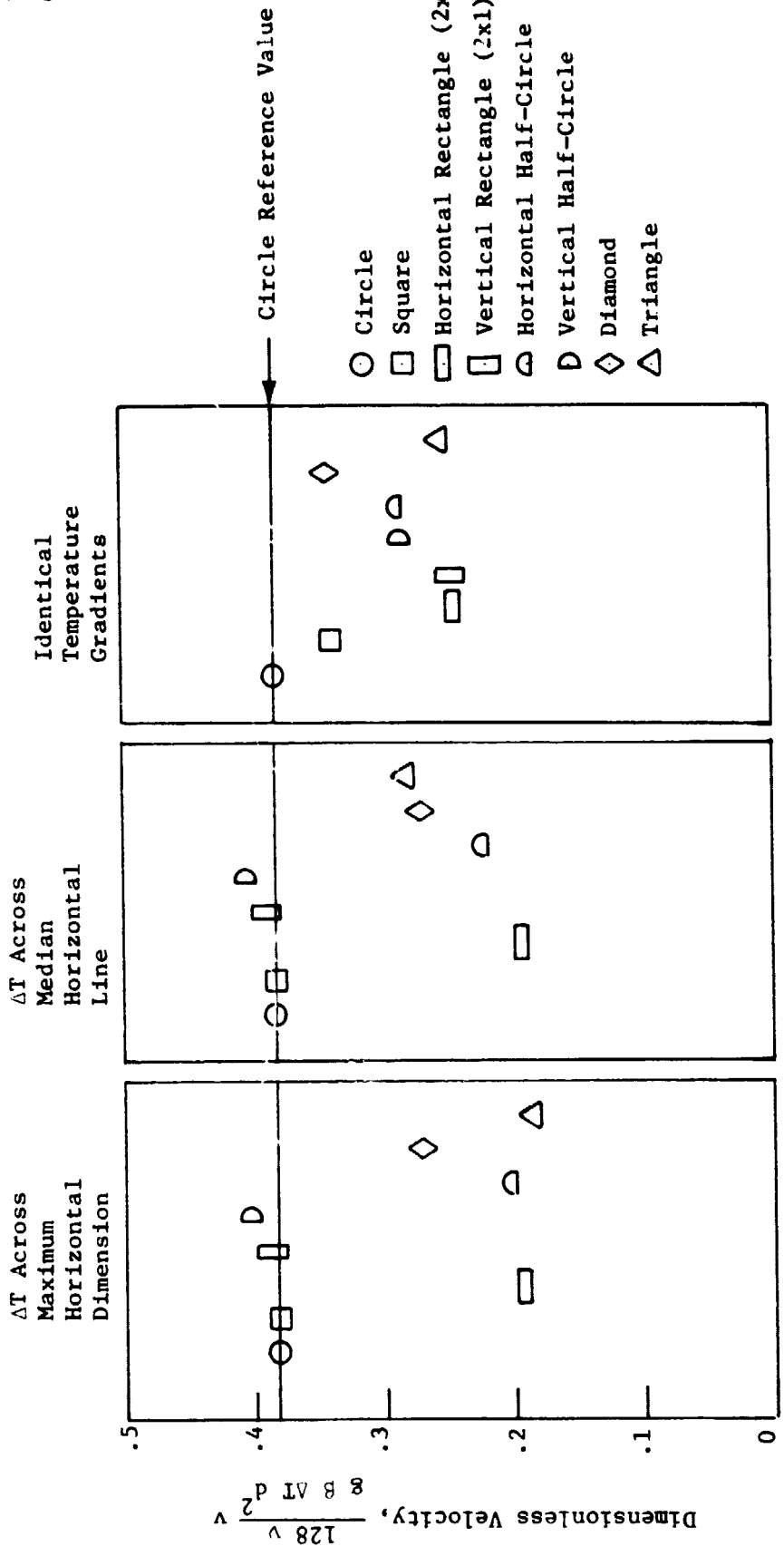

Fig. 9 - Comparison of Steady State Velocities for Natural Convection in Two-Dimensional Enclosures of Various Shape and Rayleigh Number of 1000

ORIGINAL PAGE IS
OF POOR QUALITY

Fig. 10 - Comparison of Steady State Velocities for Natural Convection in Two-Dimensional Enclosures of Various Shape and Rayleigh Number of 5000

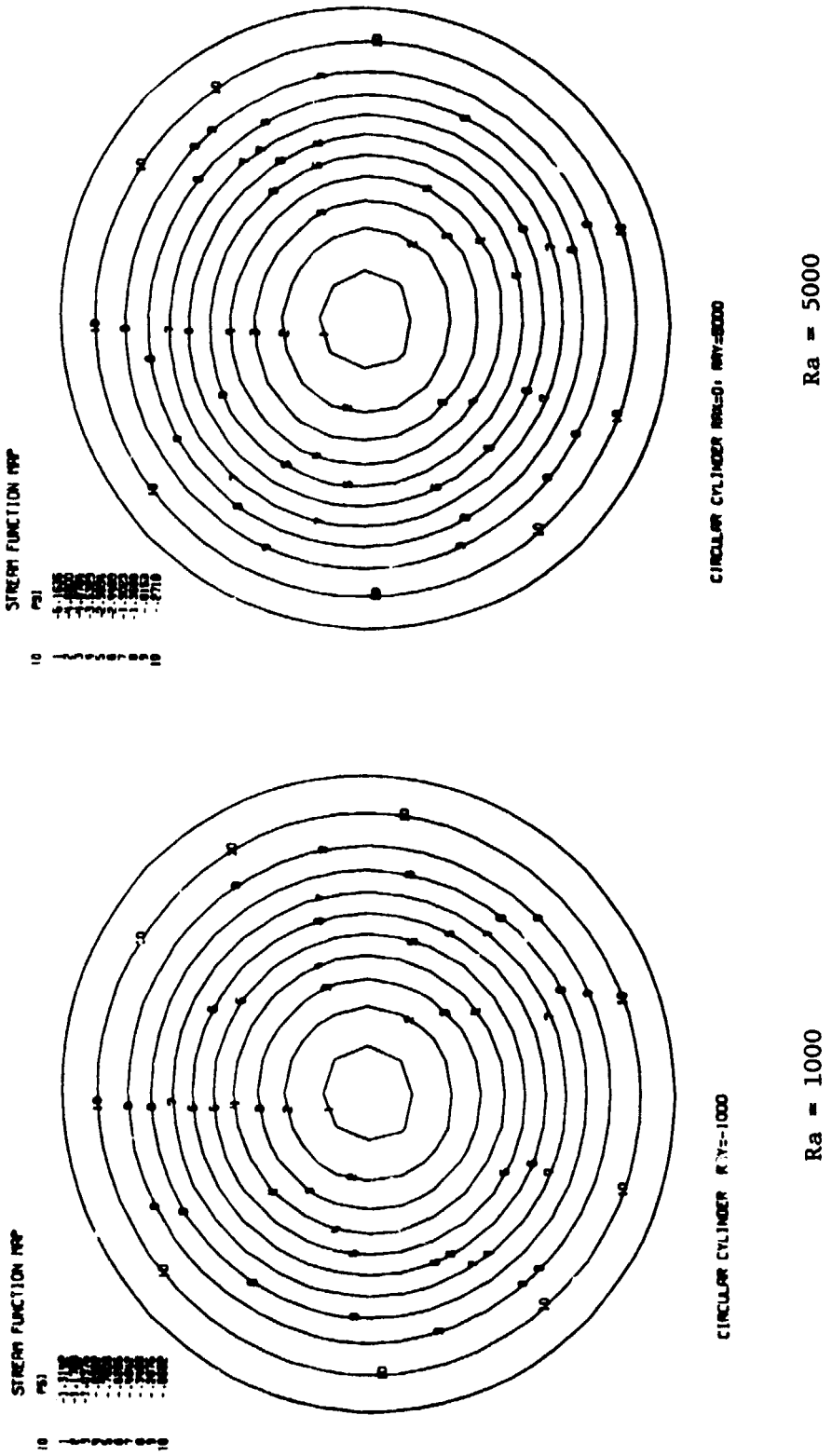

Ra = 5000

Ra = 1000

Fig. 11 - Streamline Plots for Circular Enclosure

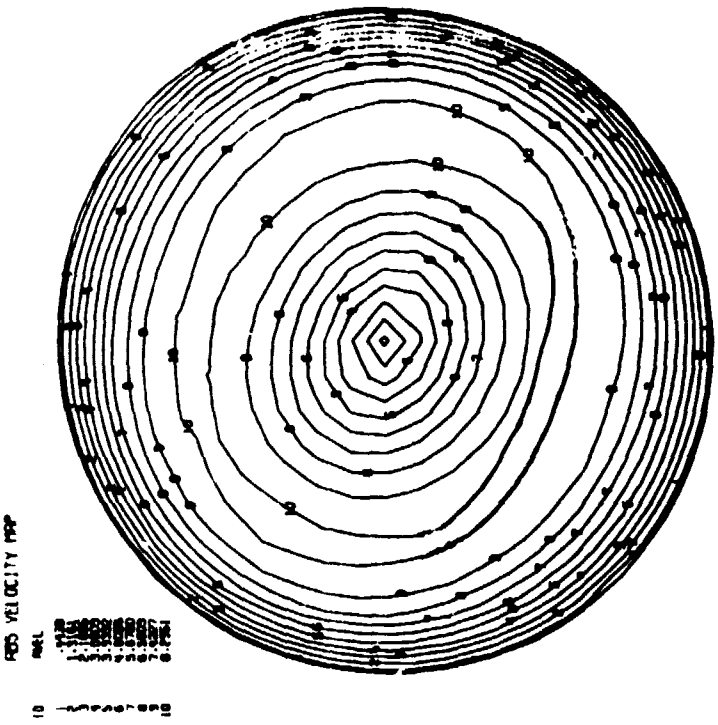

Ra = 5000

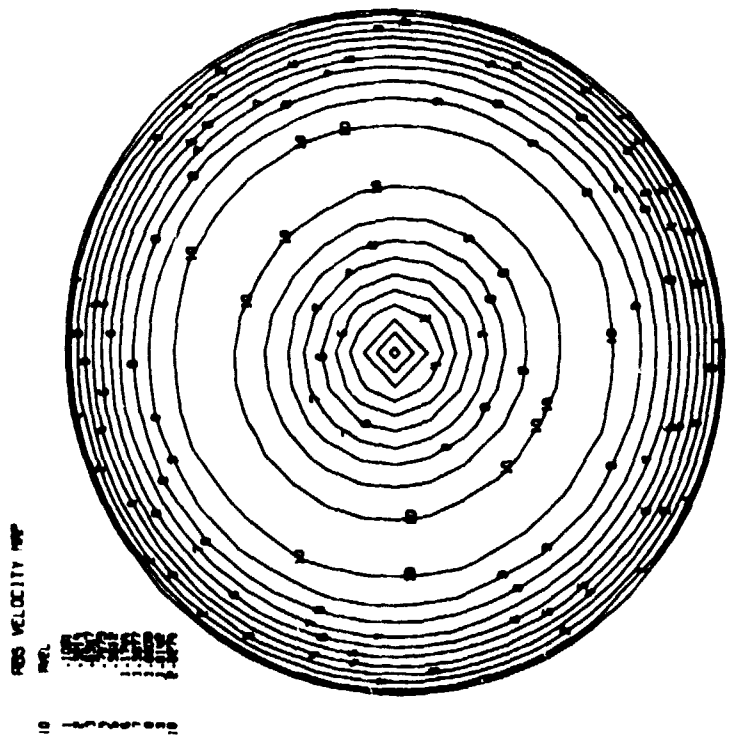

Ra = 1000

Fig. 12 - Absolute Velocity Contour Plots for Circular Enclosure

ORIGINAL PAGE IS
OF POOR QUALITY

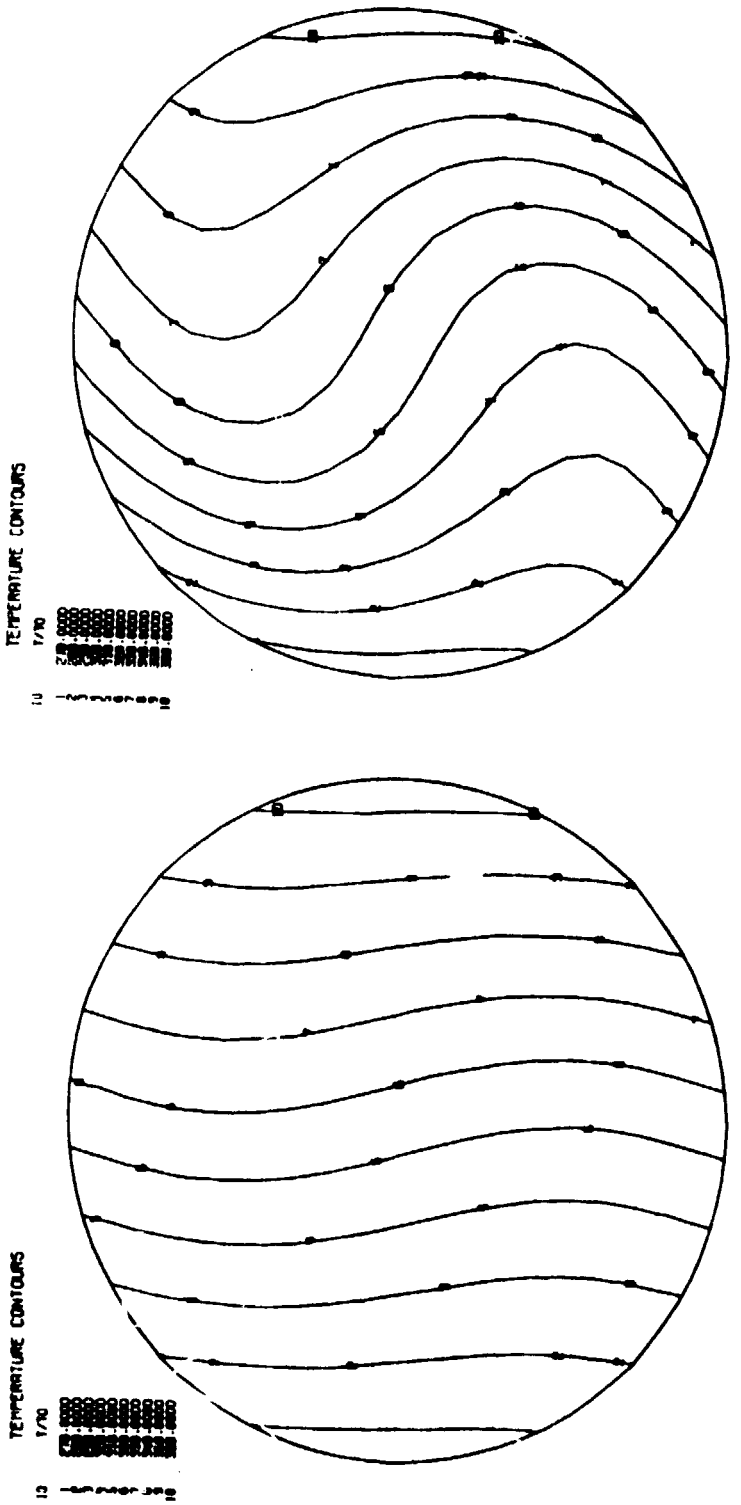

Ra = 5000

Ra = 1000

Fig. 13 - Temperature Contour Plots for Circular Enclosure

ORIGINAL PAGE IS
OF POOR QUALITY

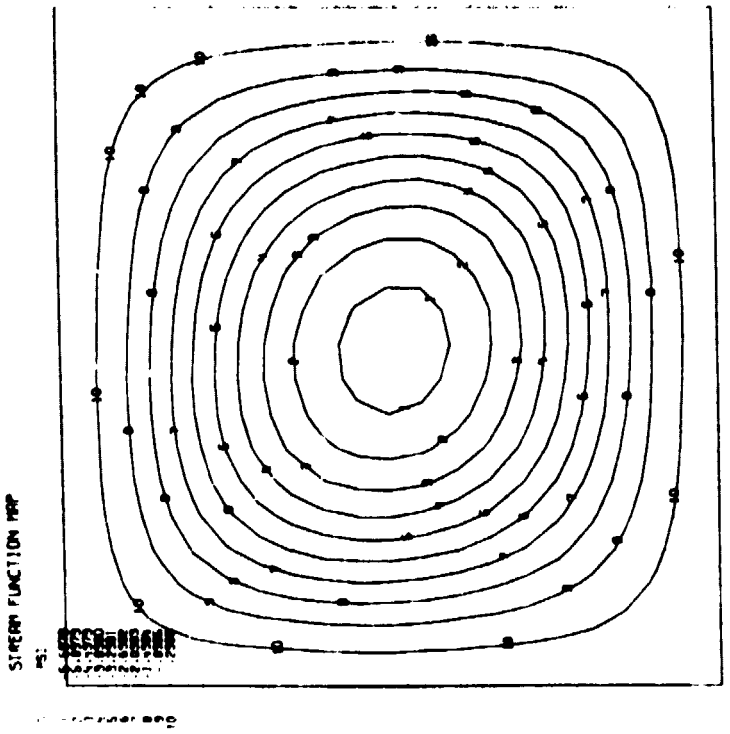

Ra = 5000

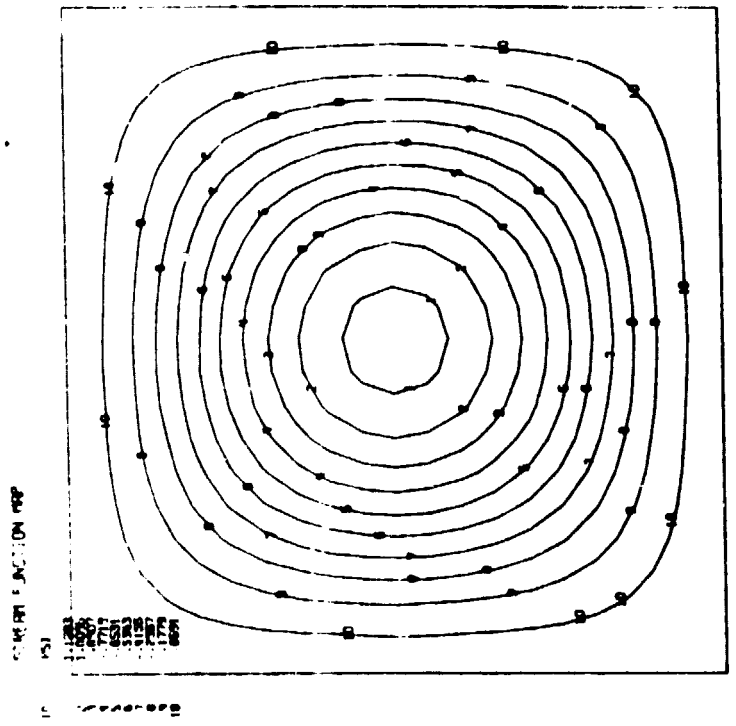

Ra = 1000

Fig. 14 - Streamline Plots for Square Enclosure

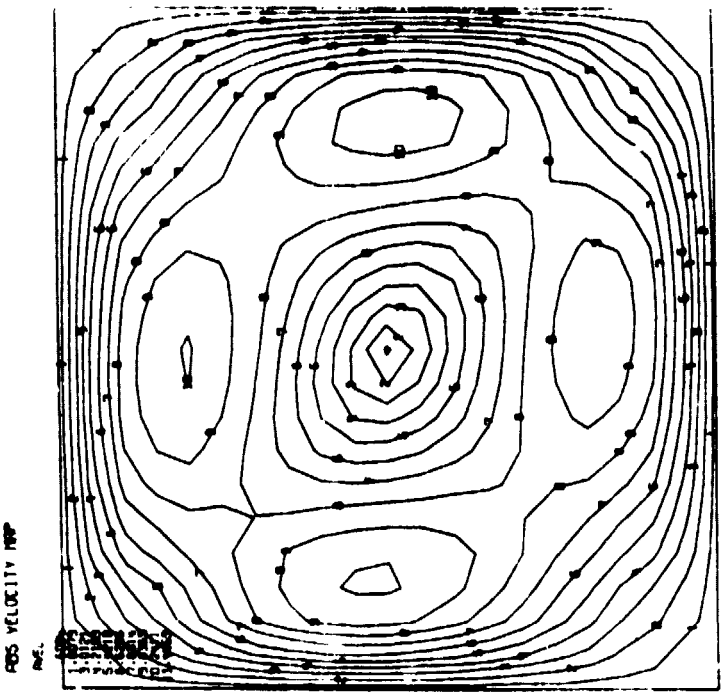

Ra = 5000

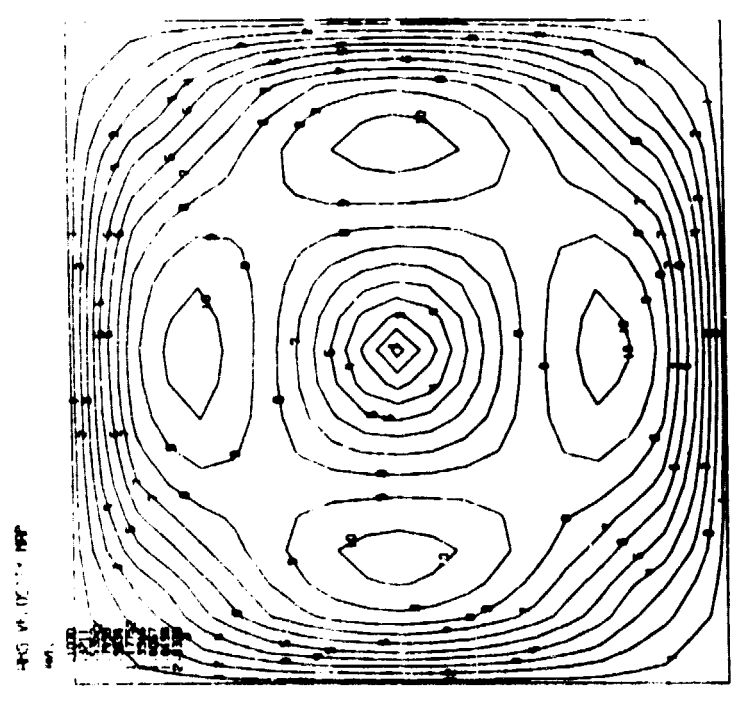

Ra = 1000

Fig. 15 - Absolute Velocity Contour Plots for Square Enclosure

ORIGINAL PAGE IS
OF POOR QUALITY

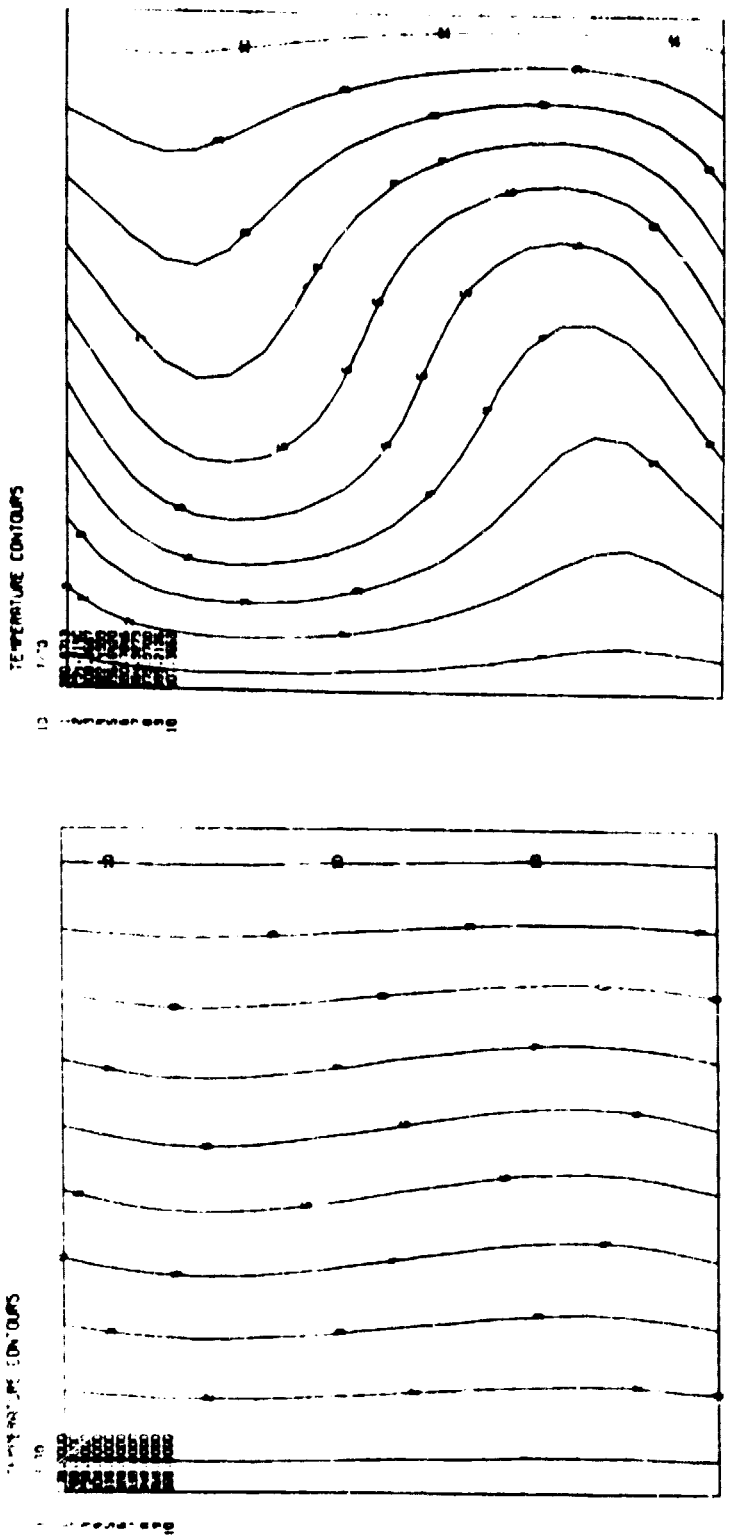

Ra = 5000

Ra = 1000

Fig. 16 - Temperature Contour Plots for Square Enclosure

ORIGINAL PAGE IS
OF POOR QUALITY

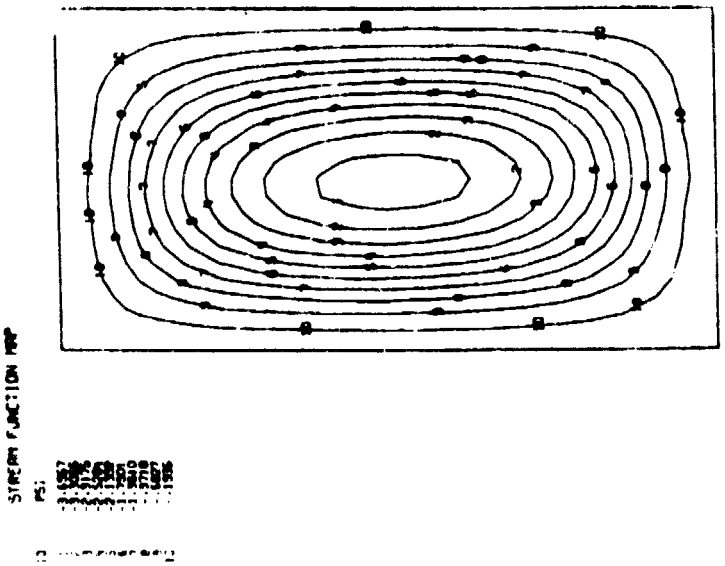

Ra = 5000

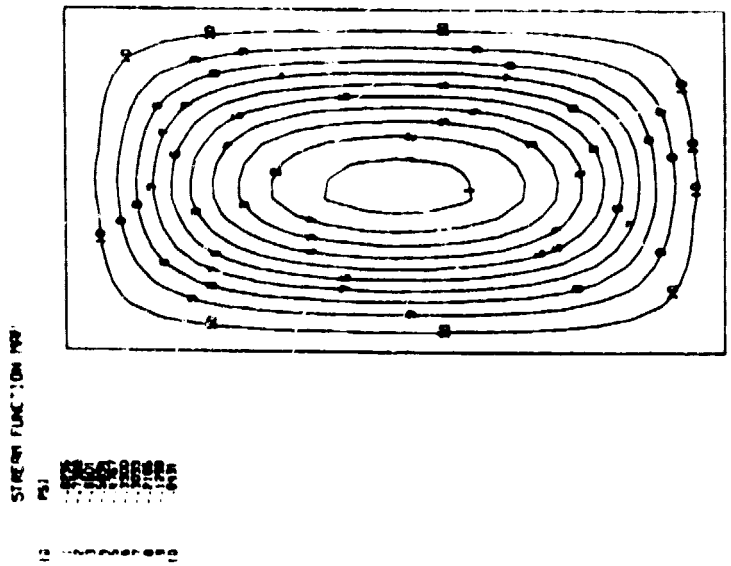

Ra = 1000

Fig. 17 - Streamline Plots for Upright 2x1 Aspect Ratio Rectangular Enclosure

ORIGINAL PAGE IS
OF POOR QUALITY

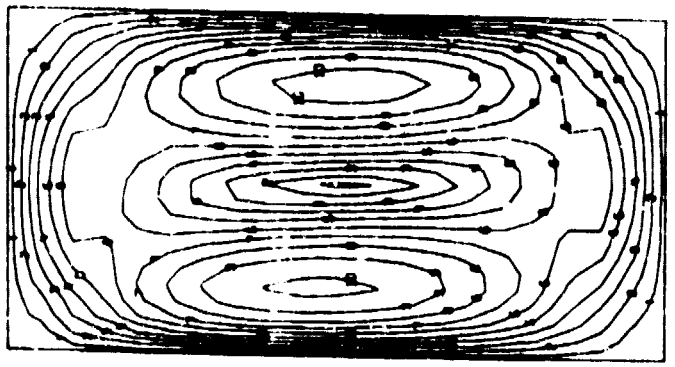

Ra = 5000

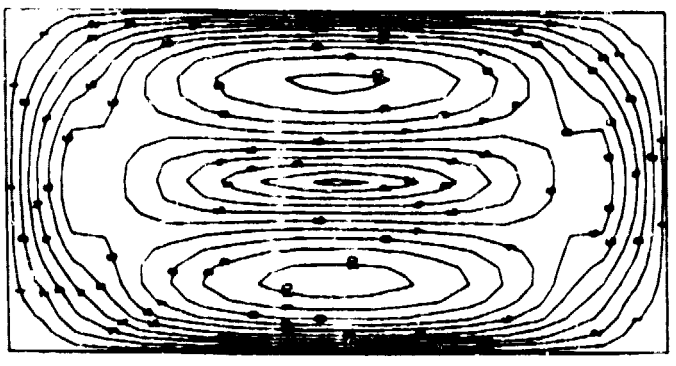

Ra = 1000

Fig. 18 - Absolute Velocity Contour Plots for Upright 2x1 Aspect Ratio Rectangular Enclosure

ORIGINAL PAGE IS
OF POOR QUALITY

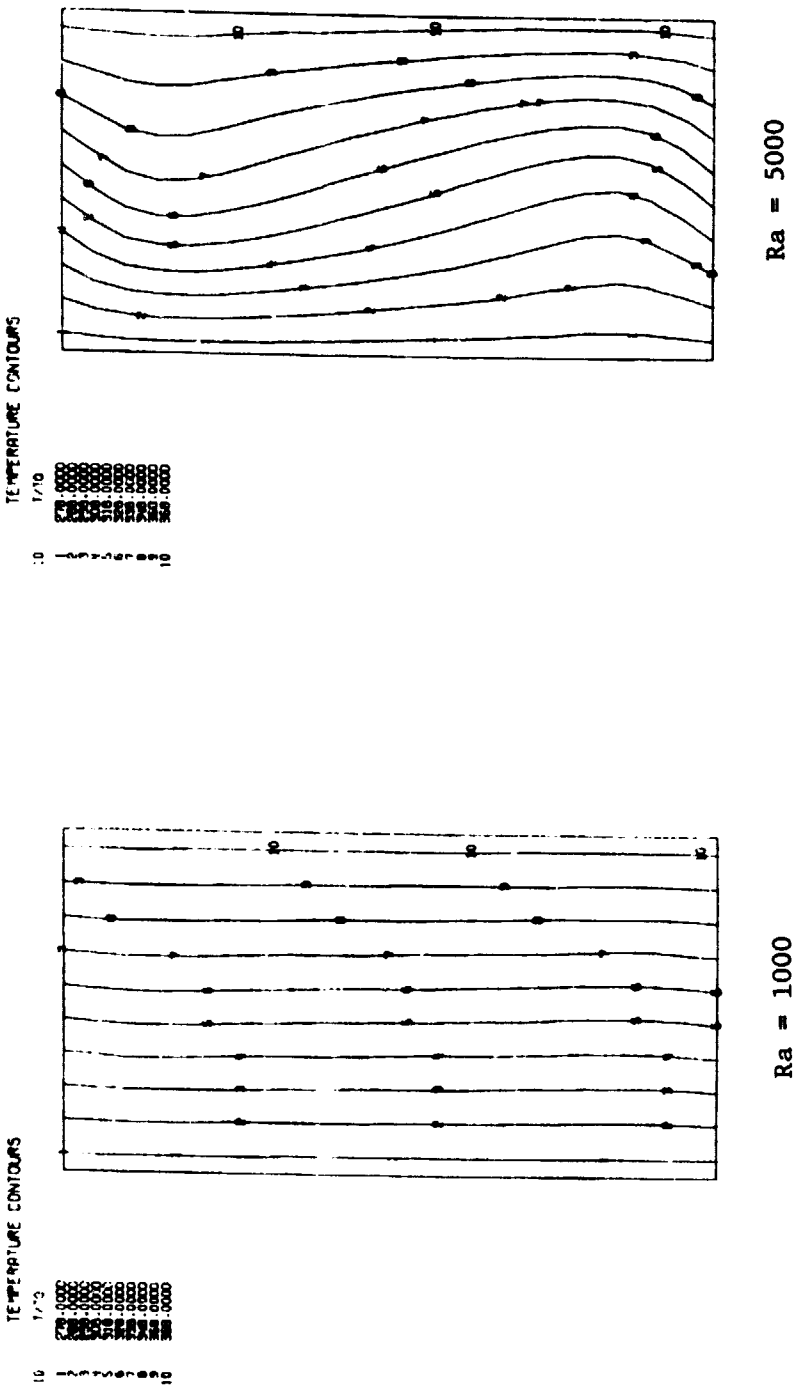

Fig. 19 - Temperature Contour Plots for Upright 2x1 Aspect Ratio Rectangular Enclosure

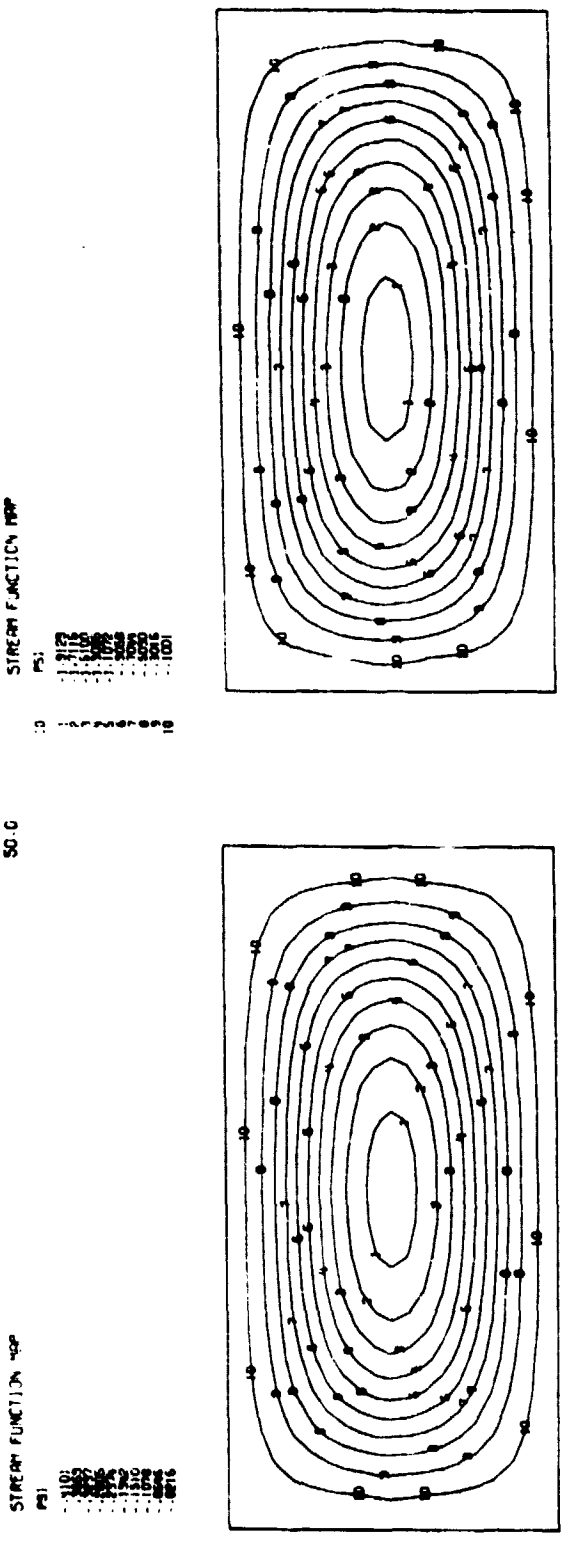

Fig. 20 - Streamline Plots for Horizontal 2x1 Aspect Ratio Rectangular Enclosure

ORIGINAL PAGE IS
OF POOR QUALITY

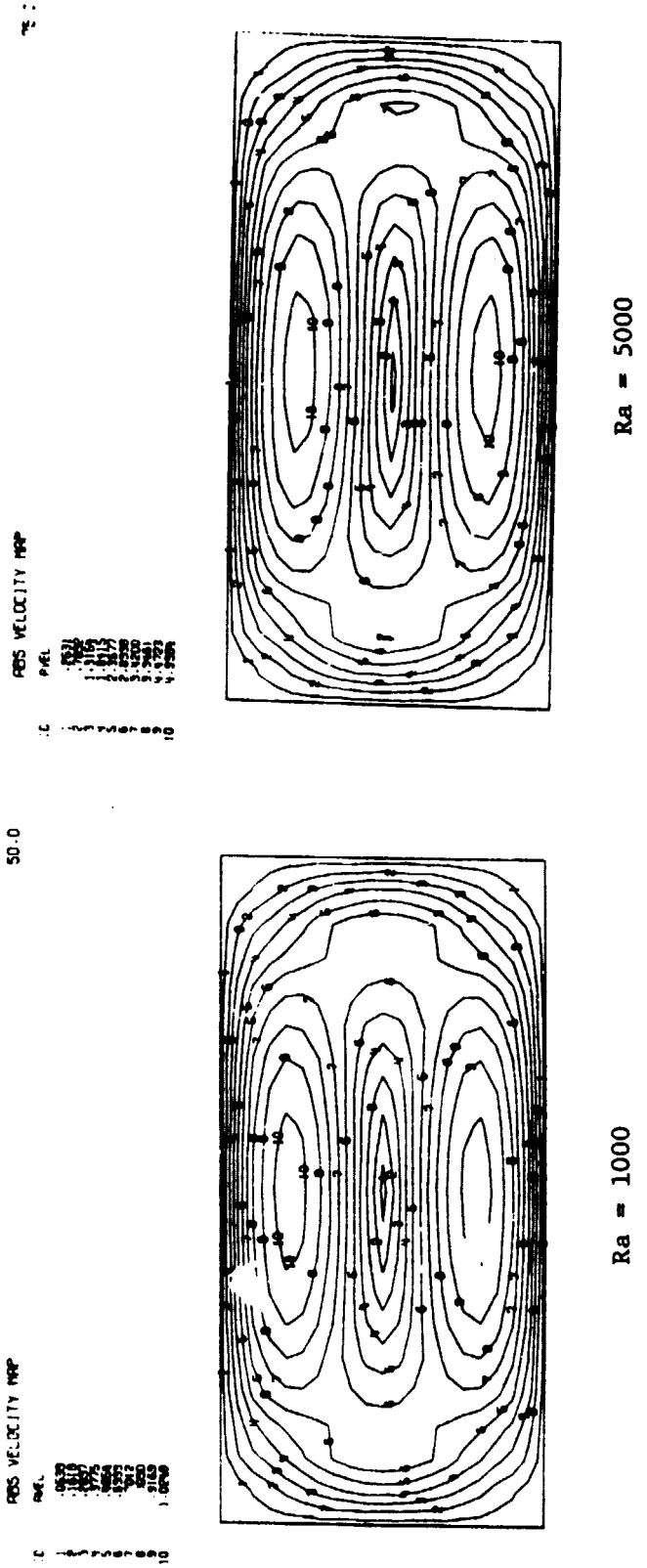

Fig. 21 - Absolute Velocity Contour Plots for Horizontal 2x1 Aspect Ratio Rectangular Enclosure

ORIGINAL PAGE IS
OF POOR QUALITY

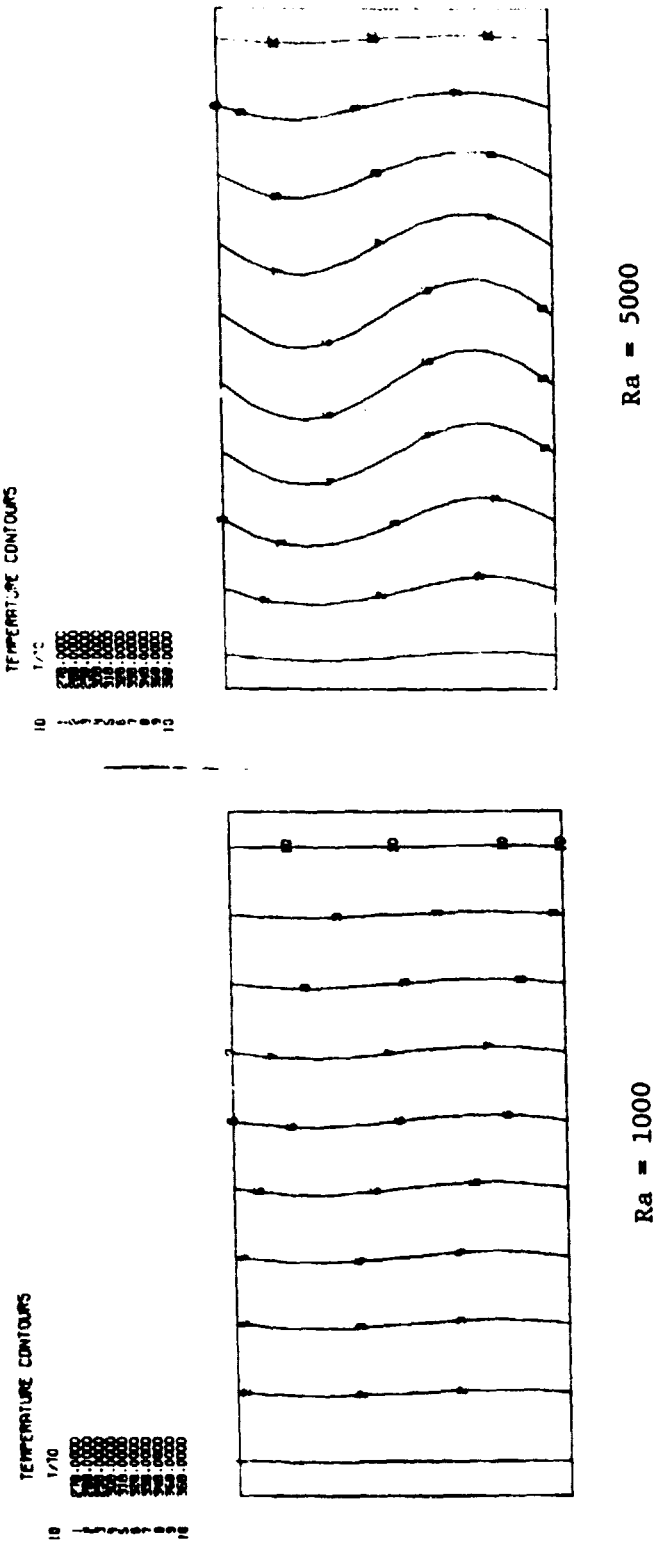

Fig. 22 - Temperature Contour Plots for Horizontal 2x1 Aspect Ratio Rectangular Enclosure

ORIGINAL PAGE IS
OF POOR QUALITY

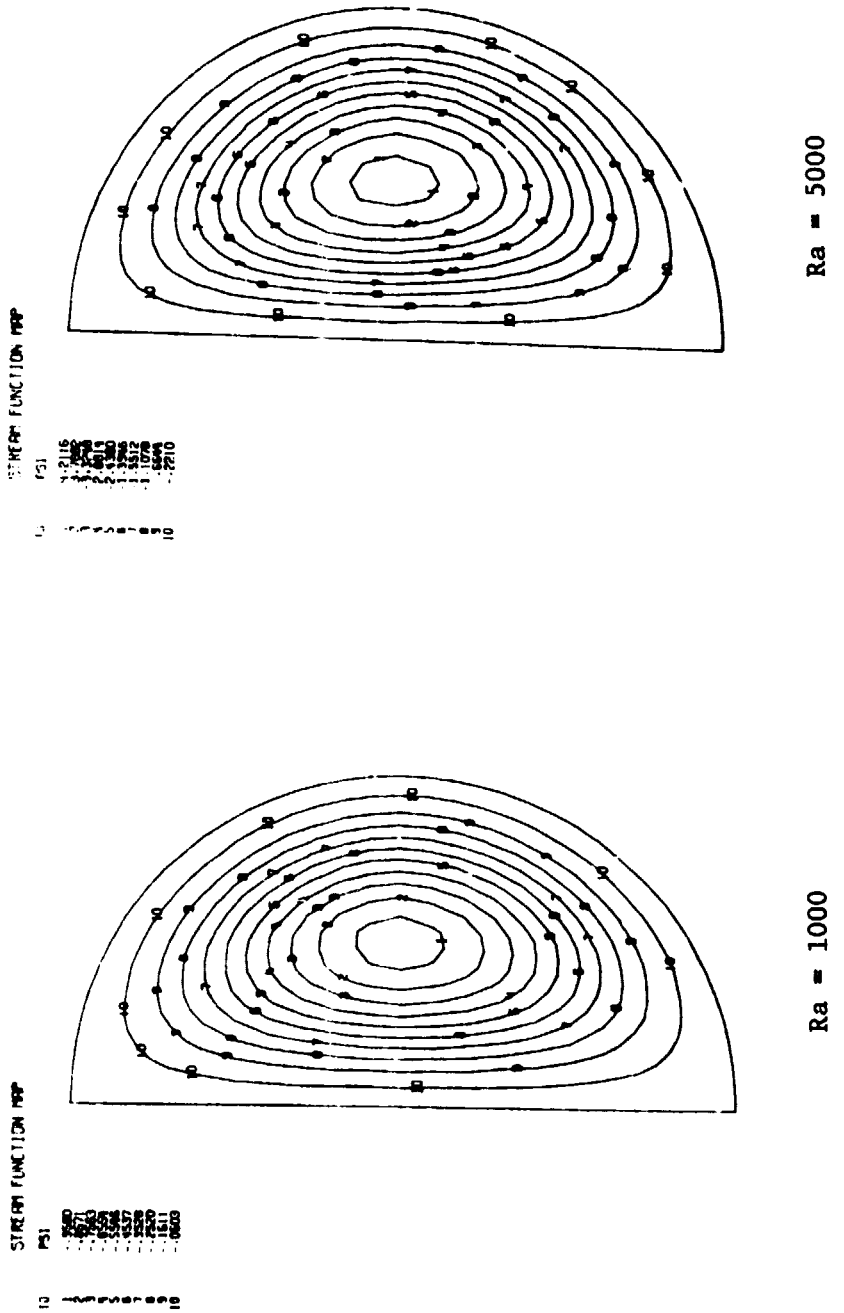

Ra = 5000

Ra = 1000

Fig. 23 - Streamline Plots for Upright Half-Circle Enclosure

ORIGINAL PAGE IS
OF POOR QUALITY

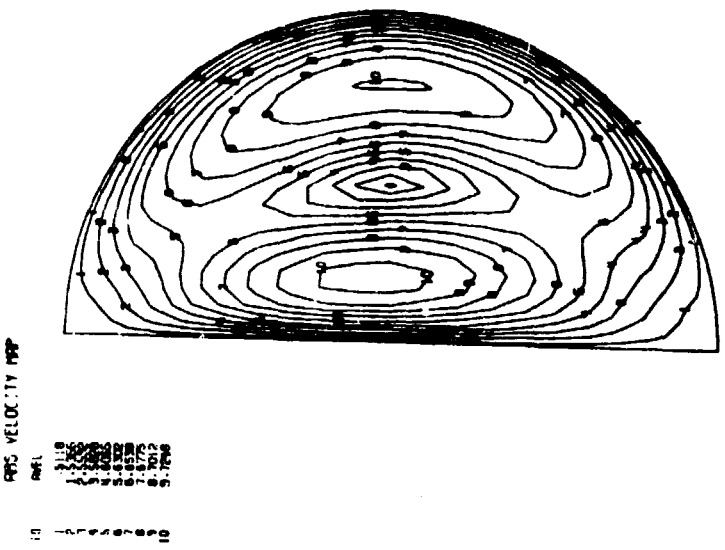

Ra = 5000

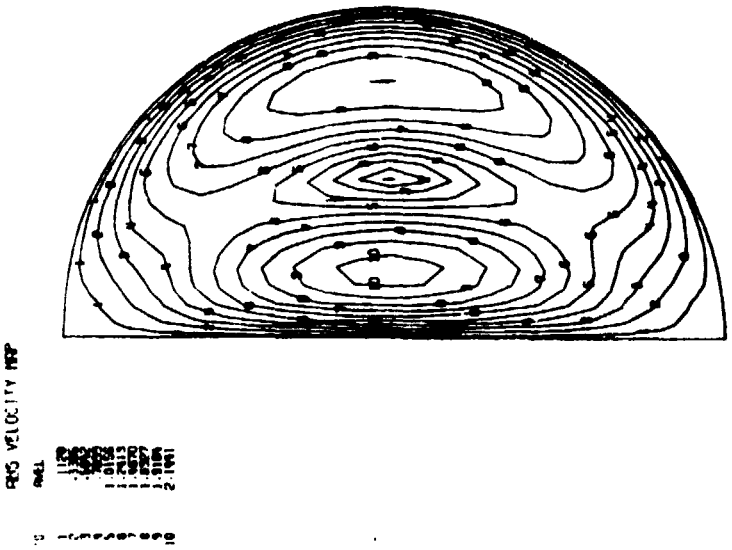

Ra = 1000

Fig. 24 - Absolute Velocity Contour Plots for Upright Half-Circle Enclosure

ORIGINAL PAGE IS
OF POOR QUALITY

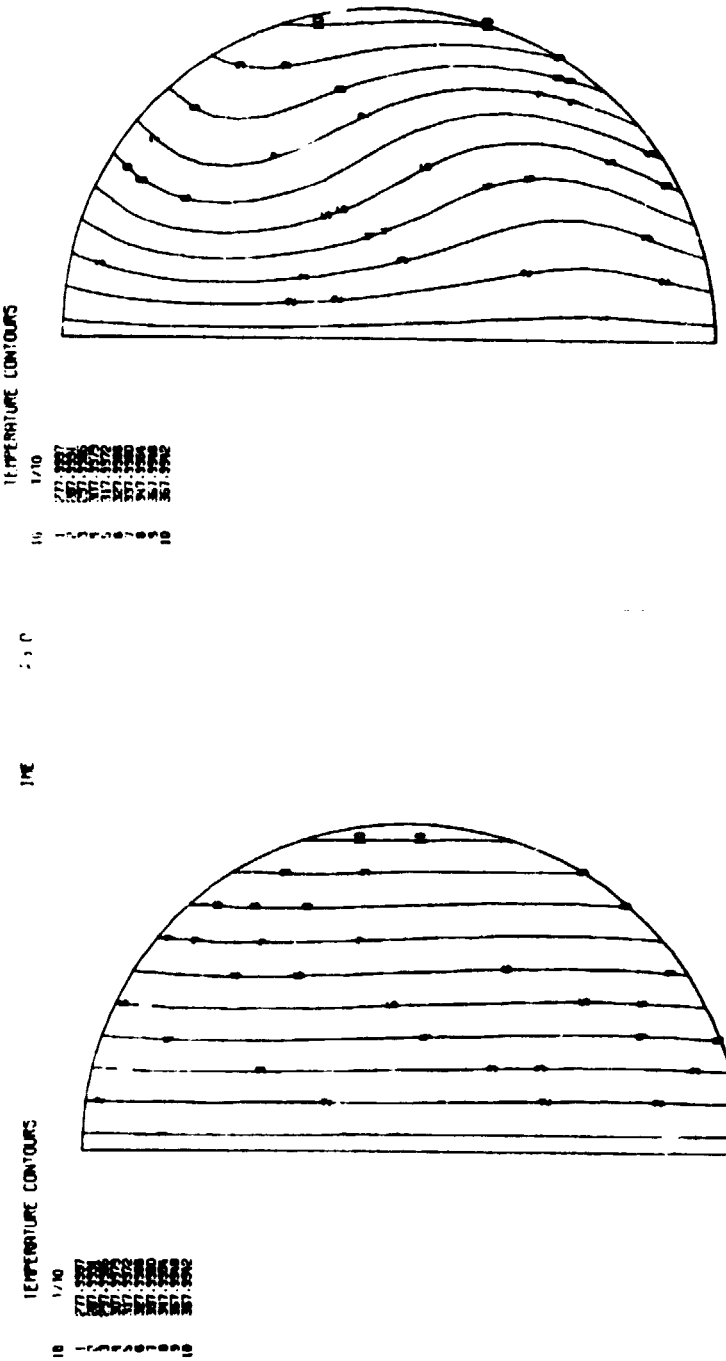

Fig. 25 - Temperature Contour Plots for Upright Half-Circle Enclosure

ORIGINAL PAGE IS
OF POOR QUALITY

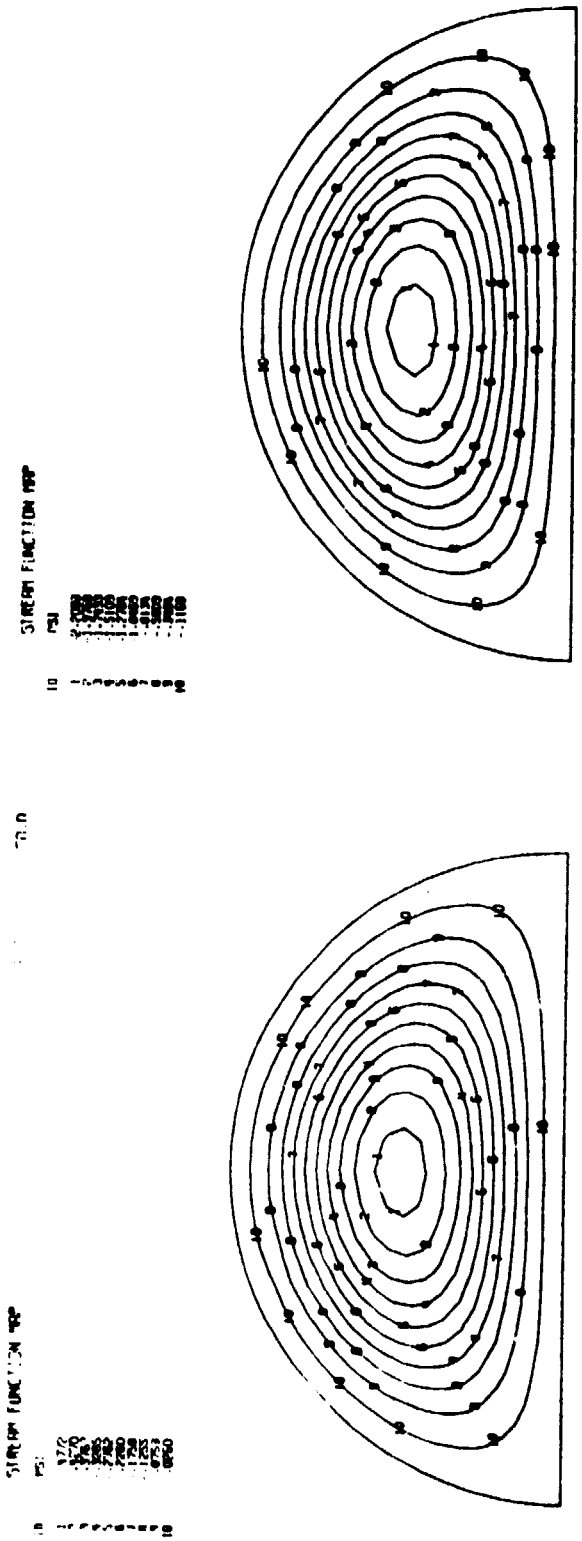

Fig. 26 - Streamline Plots for Horizontal Half-Circle Enclosure

ORIGINAL PAGE IS
OF POOR QUALITY

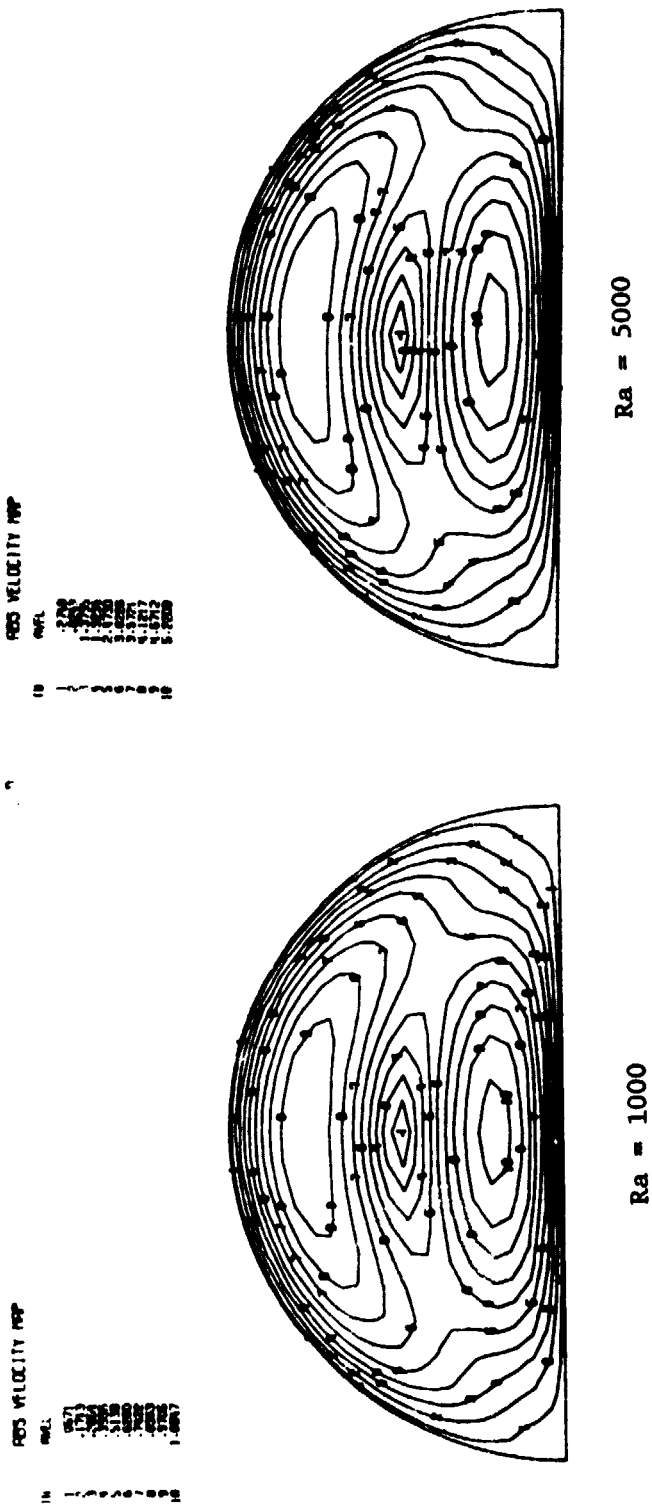

Fig. 27 - Absolute Velocity Contour Plots for Horizontal Half-Circle Enclosure

ORIGINAL PAGE IS
OF POOR QUALITY

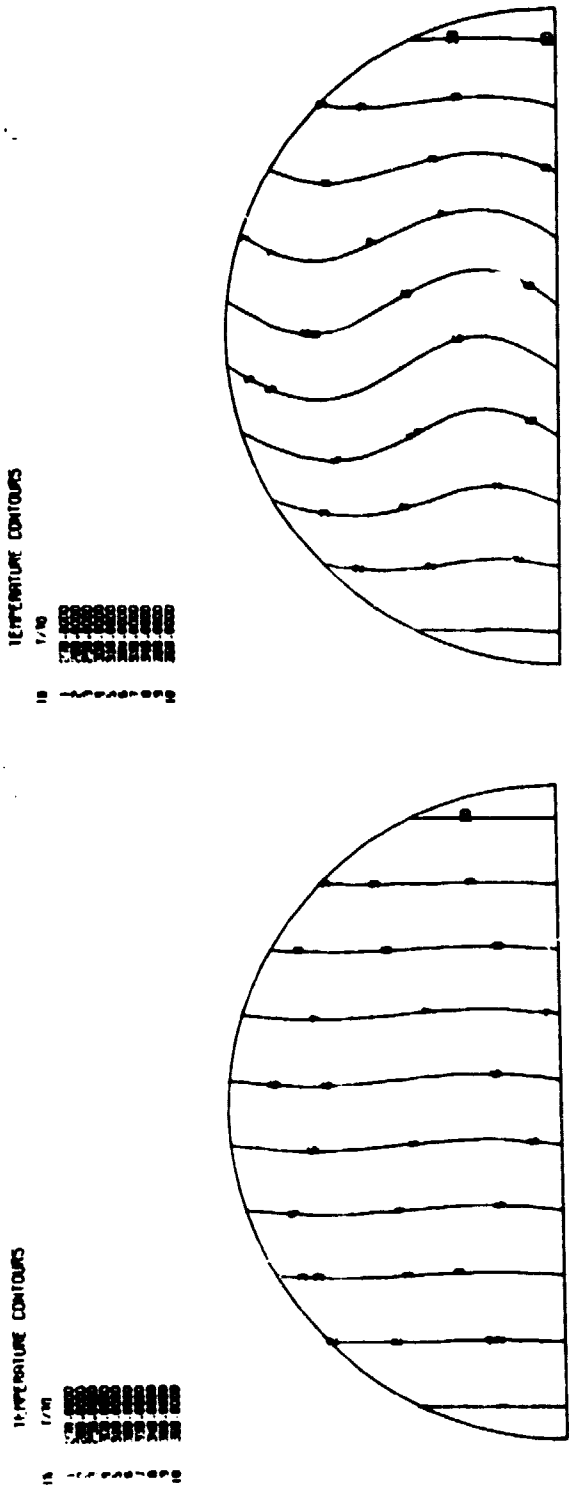

Fig. 28 - Temperature Contour Plots for Horizontal Half-Circle Enclosure

ORIGINAL PAGE IS
OF POOR QUALITY

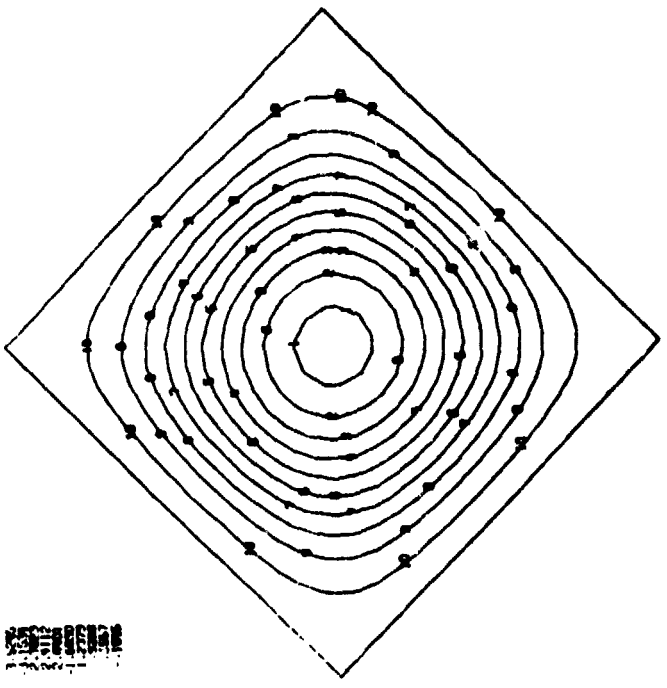

Ra = 5000

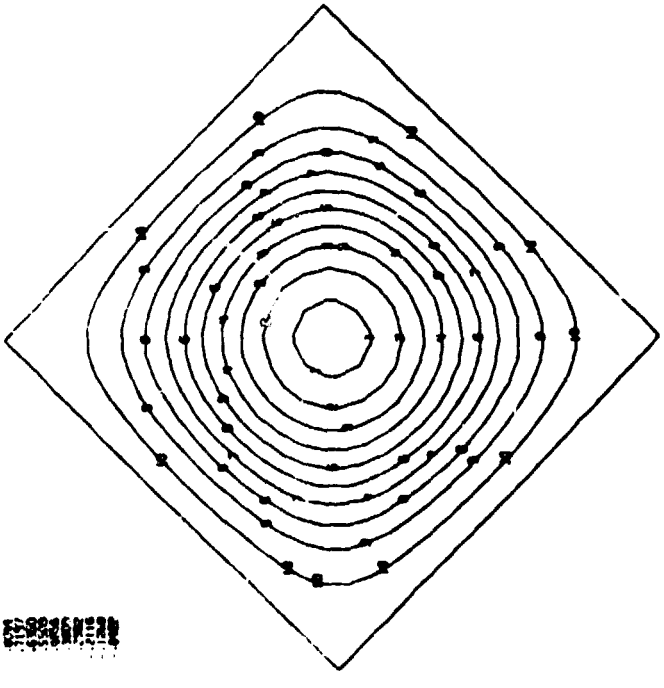

Ra = 1000

Fig. 29 - Streamline Plots for Diamond Enclosure

ORIGINAL PAGE IS
OF POOR QUALITY

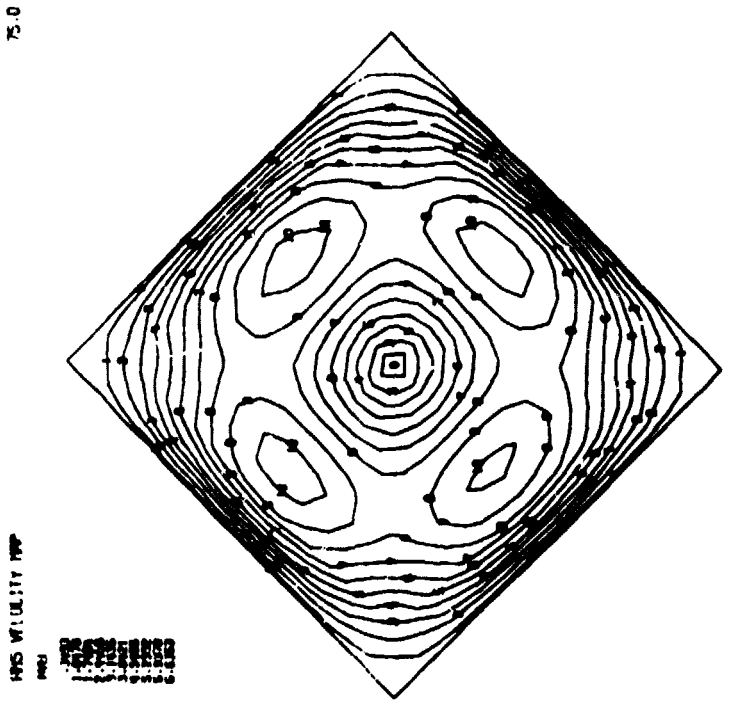

Ra = 5000

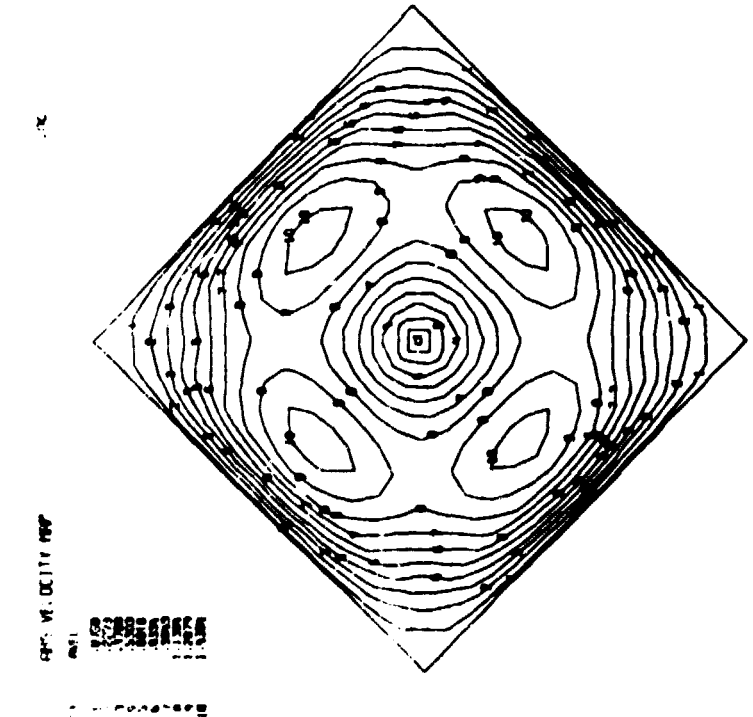

Ra = 1000

Fig. 30 - Absolute Velocity Contour Plots for Diamond Enclosure

ORIGINAL PAGE IS
OF POOR QUALITY

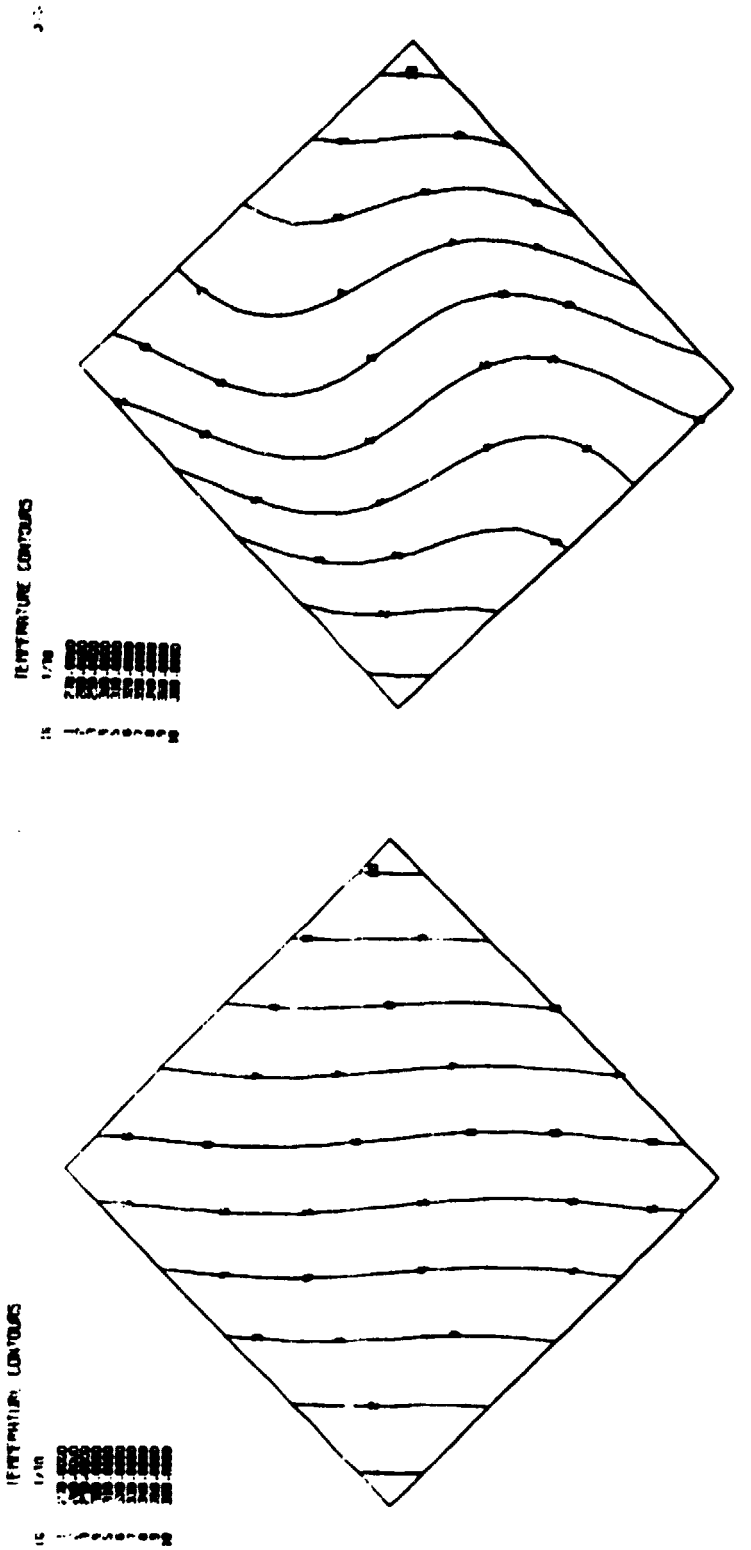

Fig. 31 - Temperature Contour Plots for Diamond Enclosure

ORIGINAL PAGE IS
OF POOR QUALITY

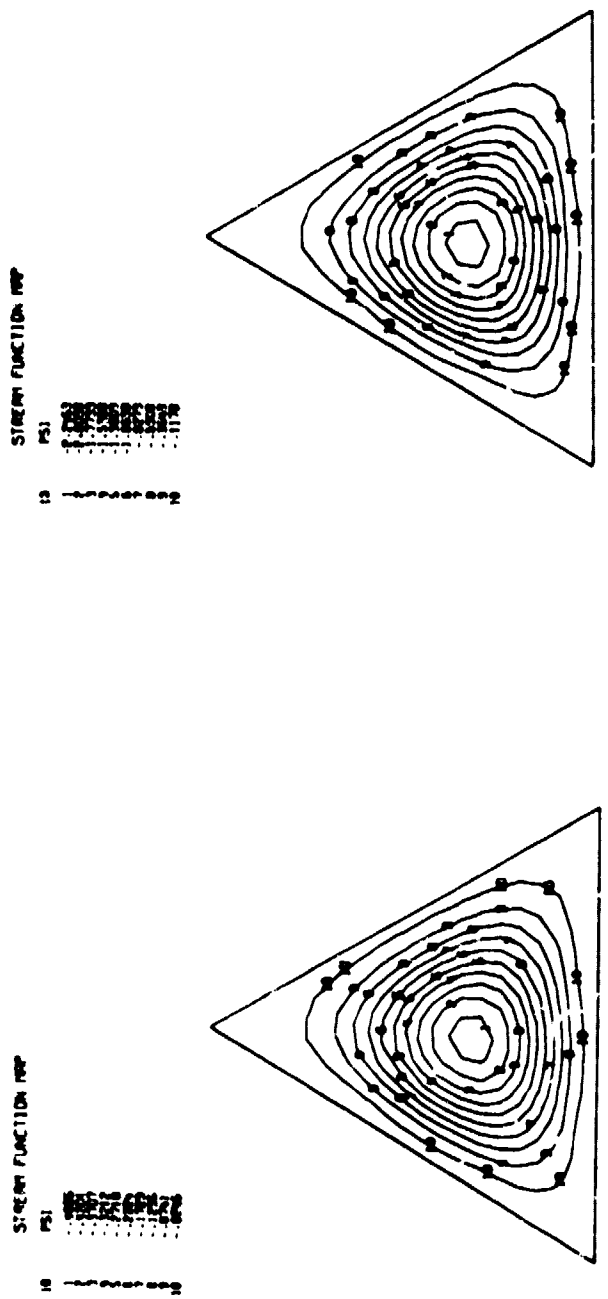

Fig. 32 - Streamline Plots for Triangular Enclosure

ORIGINAL PAGE IS
OF POOR QUALITY

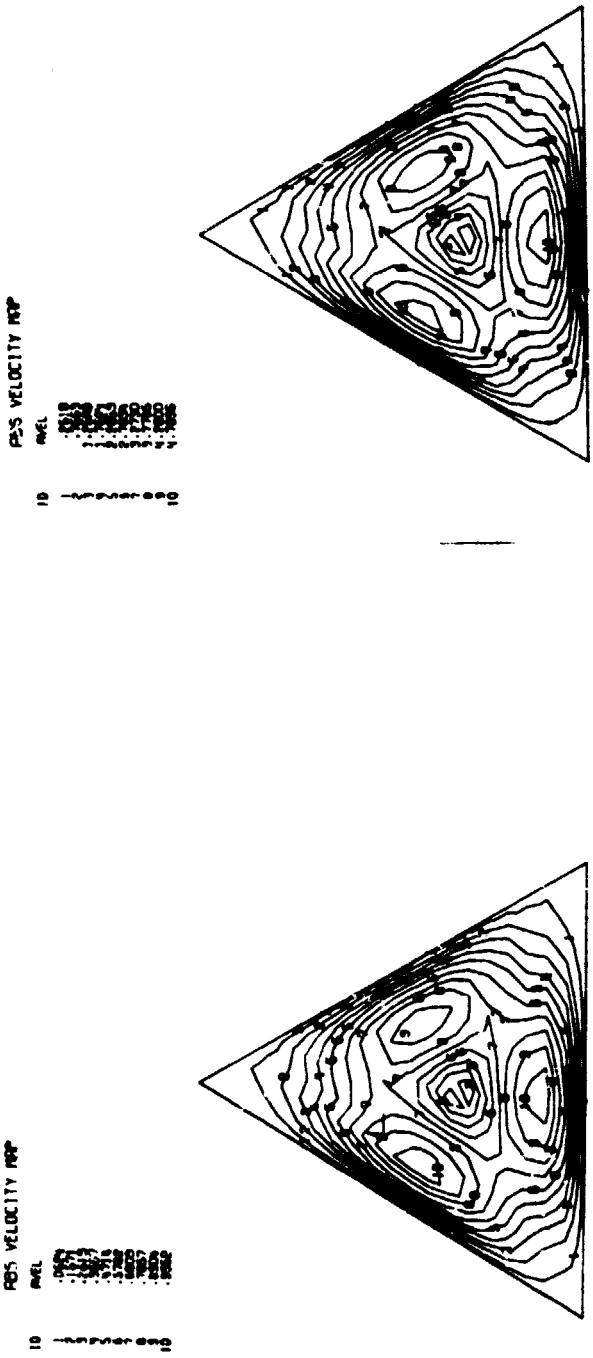

Ra = 5000

Ra = 10^0

Fig. 33 - Absolute Velocity Contour Plots for Triangular Enclosure

ORIGINAL PAGE IS
OF POOR QUALITY

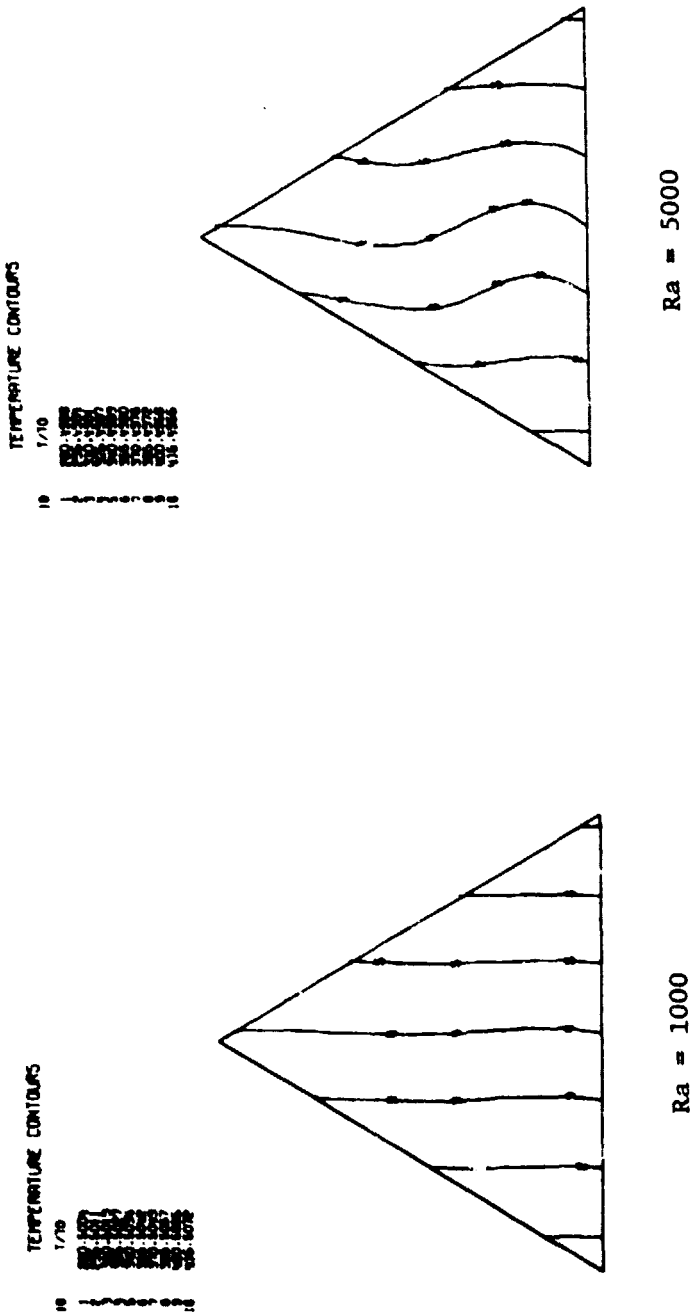

Fig. 34 - Temperature Contour Plots for Triangular Enclosure